BULLETIN OF THE EARTHQUAKE
RESEARCH INSTITUTE
UNIVERSITY OF TOKYO
Vol. 62 (1987) pp. 447-483

Report on DELP 1985 Cruises in the Japan Sea Part VII: Topography and Geology of the Yamato Basin and Its Vicinity

Masaaki KIMURA[1], Takaaki MATSUDA[2], Hiroaki SATO[3], Ichiro KANEOKA[4], Hidekazu TOKUYAMA[5], Shinichi KURAMOTO[5] Atsushi OSHIDA[1], Kiyoshi SHIMAMURA[6], Kensaku TAMAKI[5], Hajimu KINOSHITA[7] and Seiya UYEDA[4]

[1] College of Science, University of the Ryukyus
[2] Faculty of General Education, Himeji Institute of Technology
[3] Faculty of Integ. Earth and Sci., Hiroshima University
[4] Earthquake Research Institute, University of Tokyo
[5] Ocean Research Institute, University of Tokyo
[6] Faculty of Agriculture, Kyushu Tokai University
[7] Faculty of Science, Chiba University

(Received October 23, 1987)

Abstract

Topographic and geologic surveys by means of a PDR, seismic multi-channel and a dredger during the DELP-85 WAKASHIO cruise revealed that a buried ridge, tentatively named the Yamato Basin Ridge (YBR), is located in the central part of the Yamato Basin. Basalt dredged from the YBR is similar to the marginal basin basalt (MBB) and gave a K-Ar age of 7.3 ± 0.5 Ma. It supports the existence of the oceanic crust of the marginal basin type beneath the central part of the Yamato Basin. The YBR may be an extinct spreading center and is laterally offset by transverse faults. They should have been transform faults in origin once when the YBR was formed by the spreading. Sedimentary structure of probable Late Miocene and its younger sediments above the acoustic basement suggests that the spreading has not occurred since deposition of the sediments. Folds and thrusts recognized on the continental slope at the eastern margin of the Yamato Basin show that the area has been controlled under the compressive stress of which the maximum principal axis runs in a WNW-ESE direction.

1. Introduction

The DELP-85 WAKASHIO cruise was carried out by the WAKASHIO MARU (493 ton) chartered from the Nippon Salvage Company from 15 July to 3 August, 1985. This report is concerned with the topographic and seismic reflection surveys and dredge hauls conducted during the cruises. Fig. VII-1 shows the track lines of PDR, 3.5 KHz subbottom profiler, seismic reflection profiler (single and multi-channel system; 6 channels) of air-gun and magnetic surveys. Dredge locations are also displayed in the figure.

Recent paleomagnetic studies (*e.g.* OTOFUJI *et al.*, 1985a, b) suggested that the Japan Sea Basins opened during the Middle Miocene time. KIMURA (1985) claimed to have found active spreading center in the Yamato Basin. It is the main purpose of the present cruise to clarify it and when the Yamato Basin has really opened and whether it is still

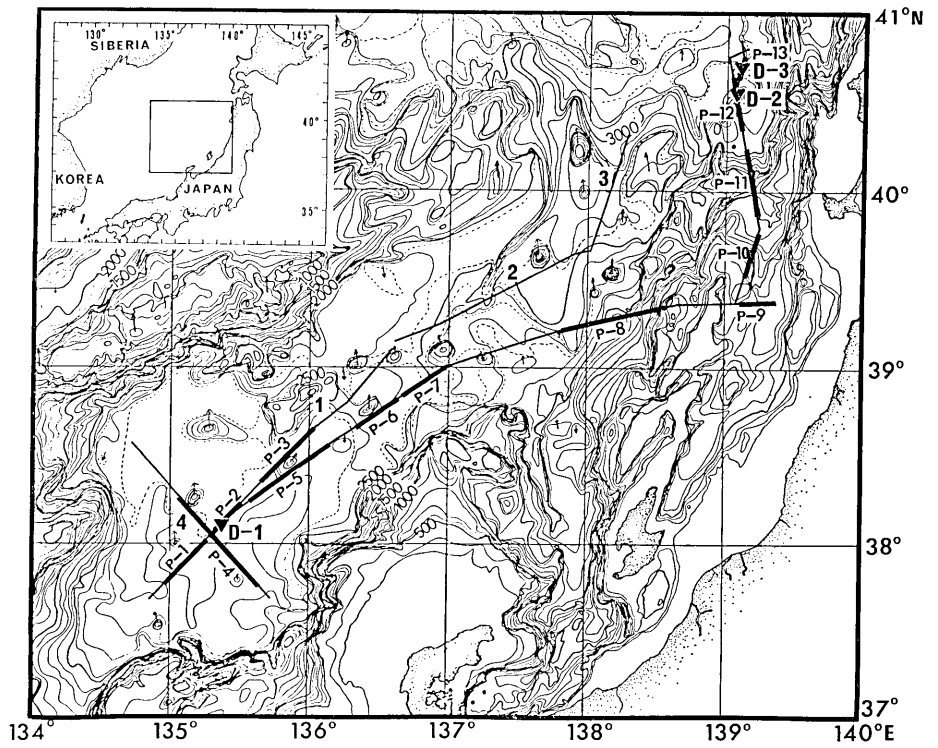

Fig. VII-1. Survey lines and locations of dredge stations (D-1—D-3) during DELP-85 WAKASHIO cruise in the Japan Sea. Inserted index map shows location of the study area. Lines 1-4 (thick letter) include multi-channel, 3.5 KHz and magnetic surveys. Others include 3.5 KHz and magnetic surveys. Thick part (P-1-P-13) shows profiling records represented in this paper. The base map is represented in Fig. VII-2.

active or not.

2. Topography

Fig. VII-2 represents the submarine topography compiled from various sources and new data obtained during the DELP-85 WAKASHIO cruise. The width of the Yamato Basin is 150–200 km and the length about 600 km subparallel to Northeast Japan. The water depth ranges between 2500–3500 meters. Many seamounts and knolls exist in the Yamato Basin. Miocene basalt was recovered from one of them during the cruise. Two

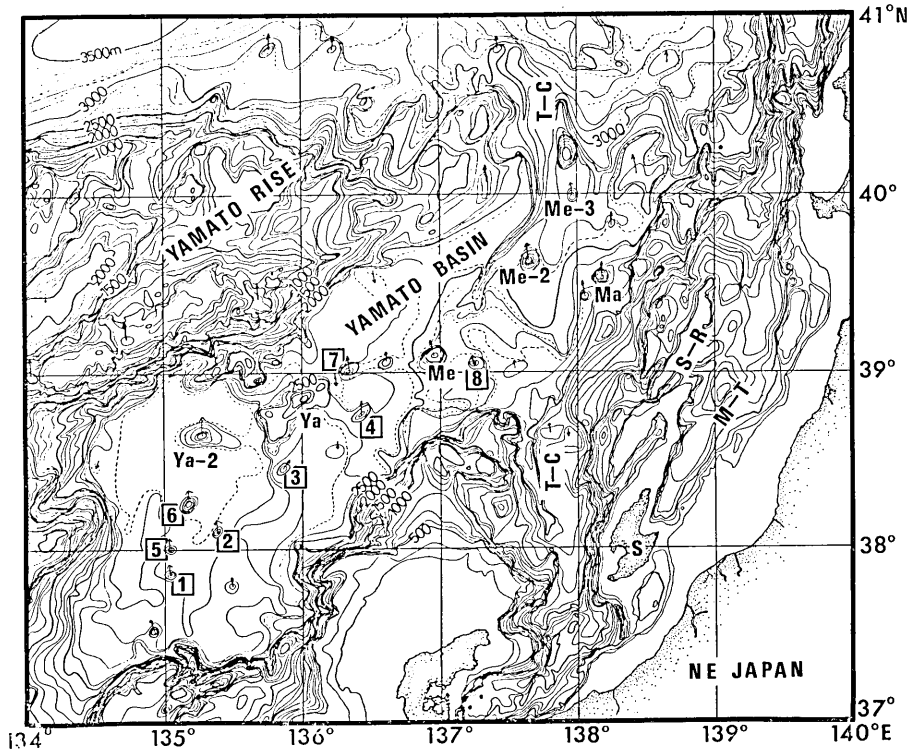

Fig. VII-2. Submarine topographic map (100 m contour interval), compiled from the charts of the Hydrographic Department, Maritime Safety Agency, Japan (1975, 1980), data obtained by the Geological Survey of Japan (1979) and those by the DELP-85 WAKASHIO cruise. 1; Yamato-85-1 Knoll*, 2; Yamato-85-2 Knoll*, 3; Yamato-85-3 Knoll*, 4; Yamato-85-4 Knoll*, 5; Yamato-85-5 Knoll*, 6; Yamato-85-6 Knoll*, 7; Yamato-85-7 Knoll*, 8; Yamato-85-8 Knoll*, Ya; Yamato Seamount, Ya-2; Yamato Second Seamount*, Me; Meiyo Seamount, Me-2; Meiyo Second Seamount, Me-3; Meiyo Third Seamount, Ma; Matsu Seamount, T-C; Toyama Deep Sea Channel, S; Sado Island, S-R; Sado Ridge, M-T; Mogami Trough. Asterisk (*) shows topographic peaks tentatively named.

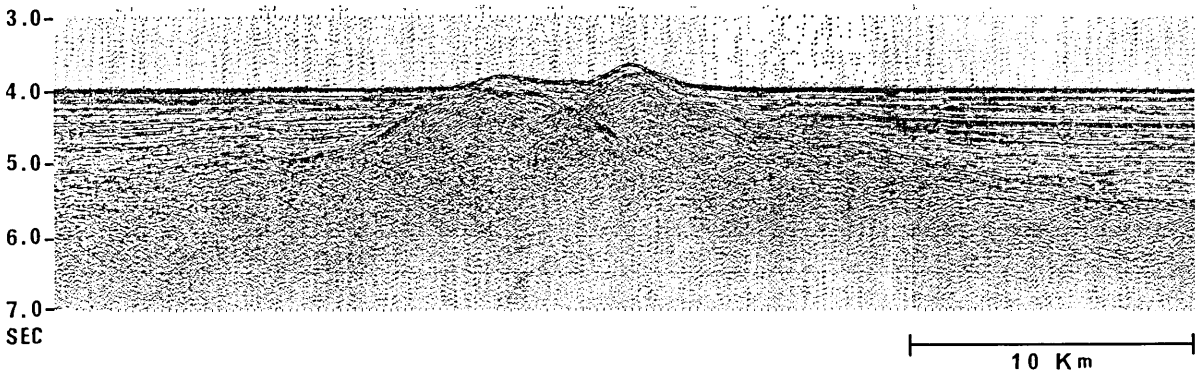

Fig. VII-3(A).

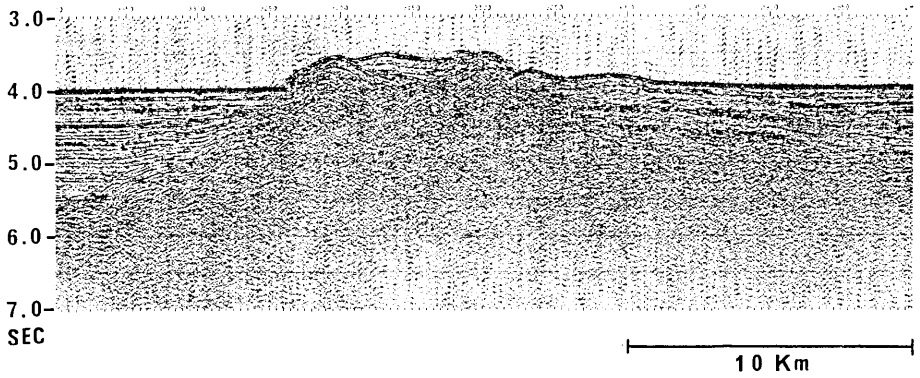

Fig. VII-3(B).

Fig. VII-3. Multi-channel profiler records showing central ridge. NE to SW from the right to the left. Two-way travel time is represented by "Sec" and so forth in other figures in this paper. Locations are shown in Fig. VII-1.
Fig. VII-3(A). P-1. Yamato-85-1 Knoll.
Fig. VII-3(B). P-2. Yamato-85-2 Knoll.

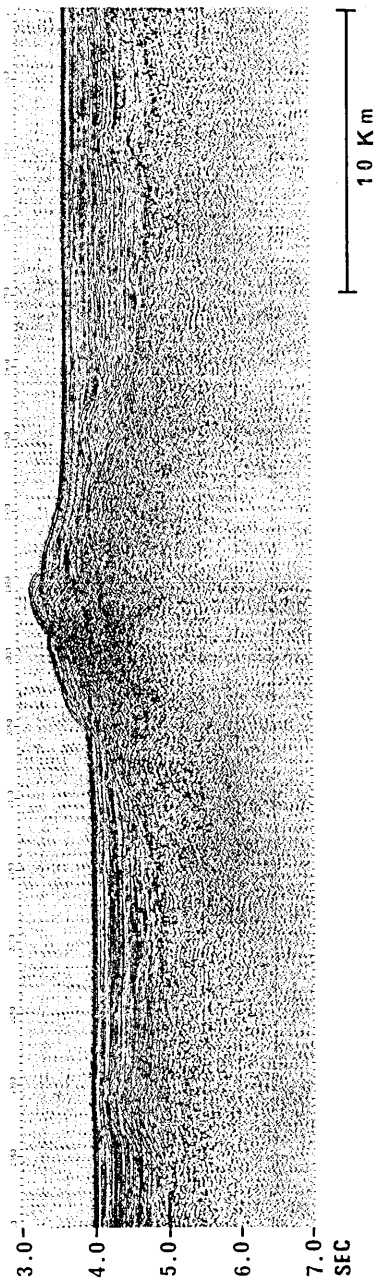

Fig. VII-3(C). P-3. Yamato-85-3 Knoll. A large difference in level can be seen between NE (right) and SW (left) sides of the knoll, suggesting a fault.

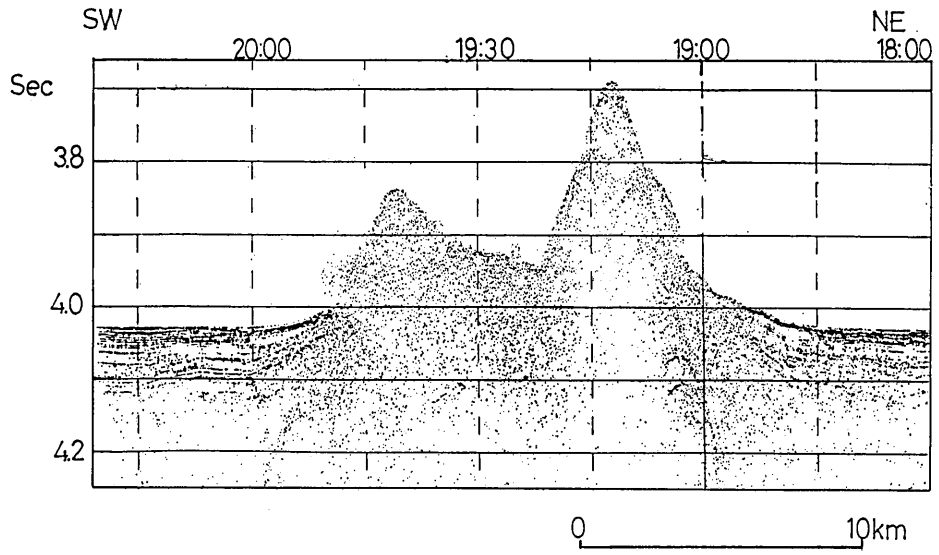

Fig. VII-4(A).

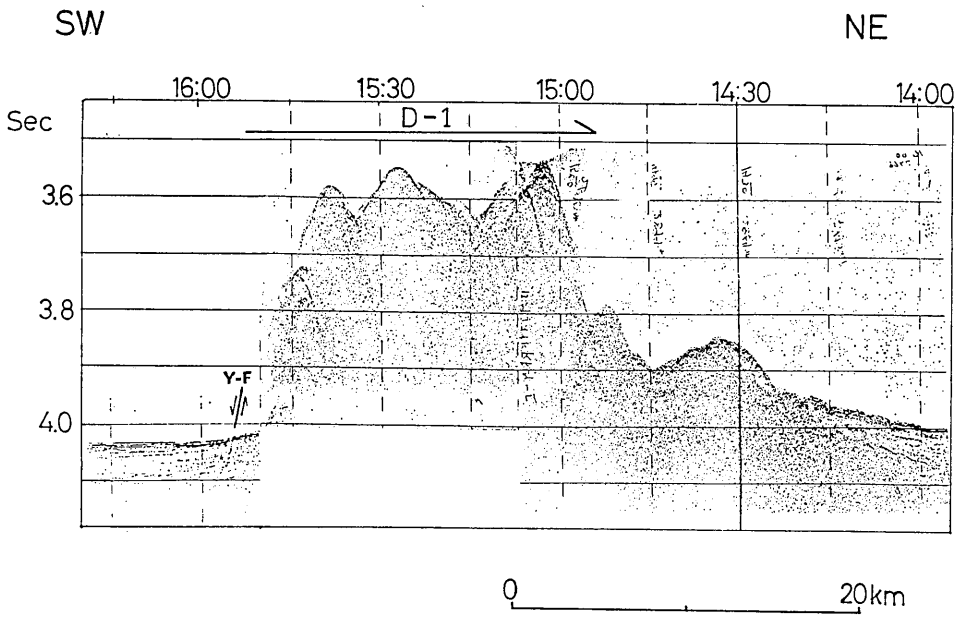

Fig. VII-4(B).

Fig. VII-4. Knolls on the YBR on 3.5 KHz records. Locations are shown in Fig. VII-1.
Fig. VII-4(A). P-1. Yamato-85-1 Knoll.
Fig. VII-4(B). P-2. Yamato-85-2 Knoll. D-1 shows location of dredging. The active normal faults (Y-F) exist as the southern foot of the knoll.

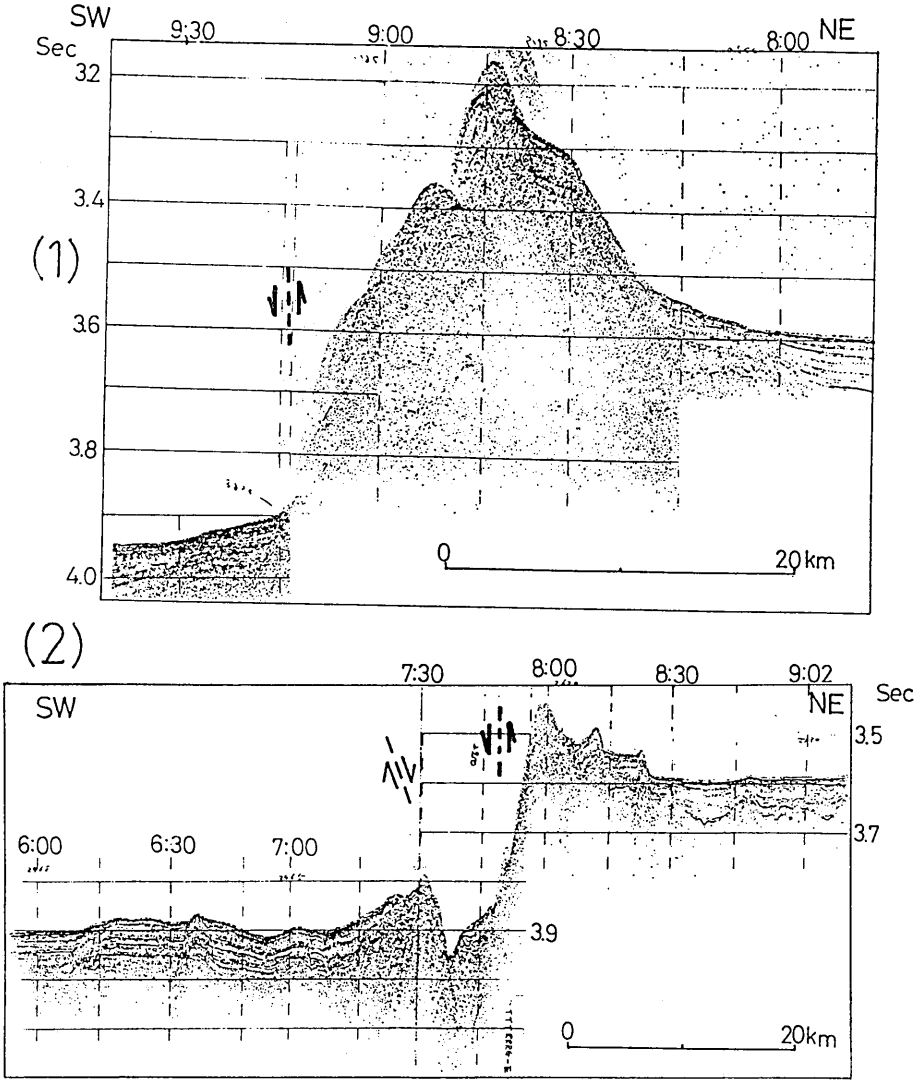

Fig. VII-4(C). Yamato-85-3 Knoll. See text for the explanation of the fault. (1) P-3. (2) P-5.

knolls were surveyed in detail by the cruise and tentatively named the "Yamato-85-1 Knoll" and the "Yamato-85-2 Knoll" (Fig. VII-2). The Yamato-85-1 Knoll has 255 m in relative height and the summit of it is 2735 m below sea level as shown on Line A (Figs. VII-3 and VII-4). The Yamato-85-2 Knoll has 395 m of relative height and its summit is 2602 m as shown on Line A (Fig. VII-4(B)). In addition, one seamount and seven knolls were tentatively named such as shown in Fig. VII-2.

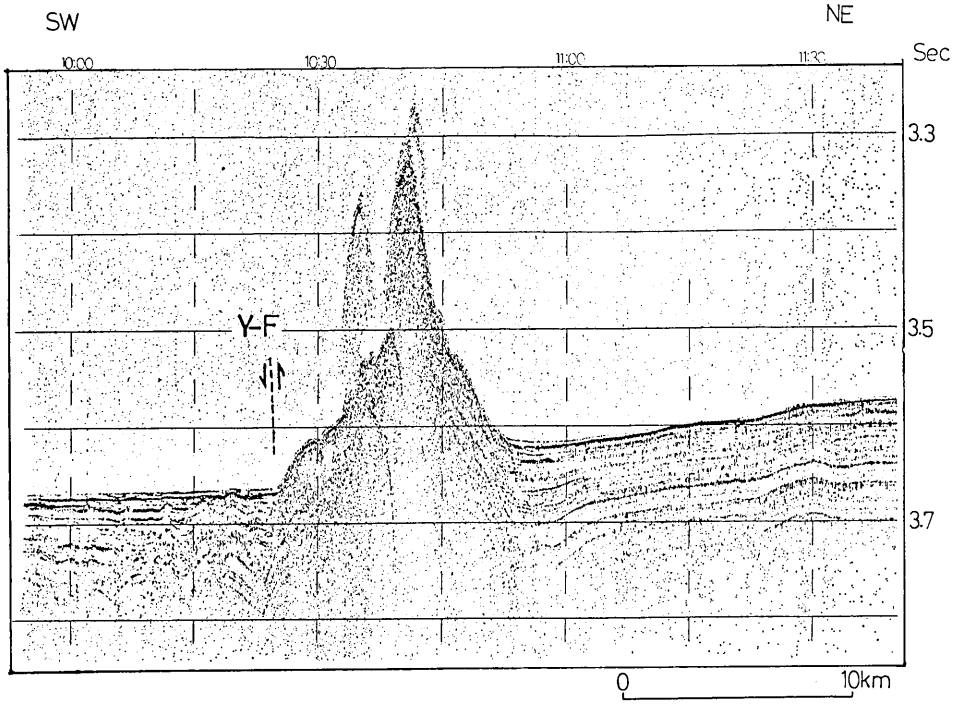

Fig. VII-4(D). P-6. Yamato-85-4 Knoll. Y-F; Young fault.

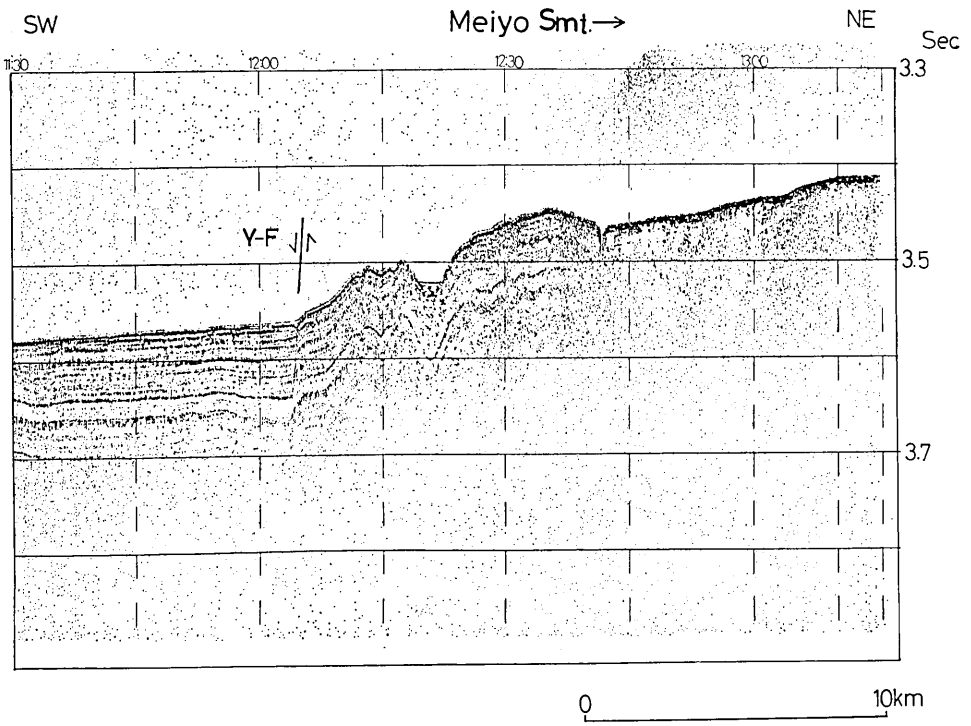

Fig. VII-4(E). P-7. Southern foot of the Meiyo Seamount. Active normal faults (Y-F) are observed.

Although they had already been shown on the profiles and submarine geologic map (GEOLOGICAL SURVEY OF JAPAN, 1979, 1981; TAMAKI, 1985, 1986), they have not been named.

As can be observed in Fig. VII-2, the seamounts and knolls appear to form two subparallel chains. The northern chain is a line of seamounts, whereas the southern chain is that of knolls on a buried basement high. We call the southern chain the Yamato Basin Ridge (YBR). The YBR is 10–20 km wide and the total length is about 400 km. The northern chain includes the Yamato-85-5 Knoll, the Yamato-85-6 Knoll, Yamato Second Seamount, Yamato Seamount and the Yamato-85-7 Knoll from the south to the north. We call it the Yamato Seamount Chain in the narrow sense because the name of the Yamato Seamount Chain hitherto includes all other seamounts in the Yamato Basin.

3. Dredged samples

Two pieces of lava and several pieces of sedimentary rocks were sampled from three stations (D-1, -2 and -3) during the cruise (Fig. VII-1; Table VII-1). The dredger used was a cylindrical chain-bag type. A semi-consolidated siltstone was recovered from D-1. The age of the sediment could not be determined paleontologically, because it contained neither nanno-plankton nor foraminifera (I. KOIZUMI, personal communication). Semi-consolidated sediments were recovered from the lowermost slope off the coast of Northeast Japan (D-2 and -3). These sediments contained Quaternary diatom which were regarded as being younger than 0.3 Ma forming a veneer of basement layers (I. KOIZUMI, personal communication).

4. Petrography of basalt

4-1. Hand specimen description

Two fragments of pillow basalt were recovered from the top of the Yamato-85-2 Knoll (D-1 site, 38°08′N, 135°24′E) (Figs. VII-3(B) and VII-4(B)). The size and weight of the fragments were $11\times7\times6$ cm and 400 g; $9\times6.5\times6.5$ cm and 330 g, respectively. The columnar joint (3–6 cm across) was well developed perpendicular to the outer surface of the pillow. The fragments showed textural variations common to pillow lavas. The chilled margin (2.5 cm thick) was yellow-gray and partly altered to palagonite. The interior of the pillow fragment was gray and showed layering structures in terms of vesicle distribution and groundmass texture (Fig. VII-5). Vesicles, about 30 vol. % of the rock, were 0.1 to 2 mm in diameter.

Table VII-1. Description of dredged samples.

Dredge Station	Date		Position		Depth (m)	Sampler	Area and Topography	
			Latitude	Longtitude				
D-1	1985 July 30	23:48 02:48	38°08.07′ 38°08.80′	135°24.12′ 135°22.27′	2348 2311	Chain bag-type Dredger	Top of the knolls (Yamato-85-2 Knoll)	◦Two pieces of basaltic pillow lava fragments. (Size; 11×7×6, 9×6.5×5.5 cm, Total weight; 730g, Color; dark gray-brown) ◦Hyaloclastite (Size; 4×3×1 cm, Weight; 10g) ◦Clay (Soft sediment; Color; brown color) ◦Subrounded pebble (Size; 1×0.5×0.8 cm, Color; light yellow) ◦Subrounded pebble (Size; 1×0.5×0.8 cm, Color; light yellow)
D-2	1985 August 2	19:13 19:12	40°33.59′ 40°34.08′	139°03.85′ 139°04.30′	3171 3210	ditto	Lower-most slope of the continental slope	◦Semi-consolicated sediment (Fine sand-silt, Size; 6×5×12 cm, Color; dark gray-gray) ◦Unconsolidated clay (Weight; 300-400g)
D-3	ditto	14:53 15:50	40°42.30′ 40°41.67′	139°06.56′ 139°06.74′	3248 3131	ditto	ditto	◦Seven pieces of semi-consolidated clay-silt (Max, Size; 3×2.5×2 cm. Color; brown-gray) ◦Unconsolidated clay (Weight; 400-500g)

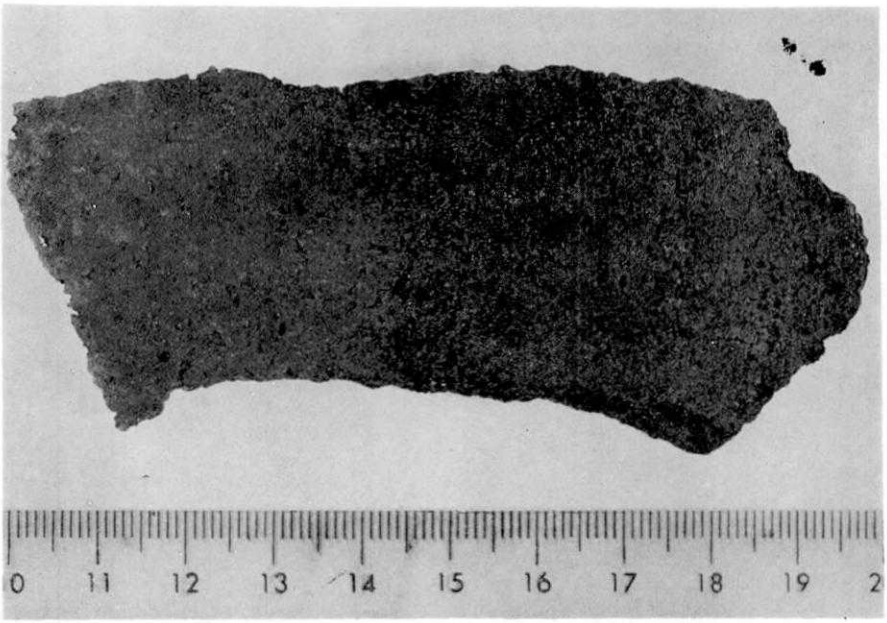

Fig. VII-5. Slab chip of D-1 basalt. Note the zonation in terms of alteration and vesicle distribution.

4-2. Thin section description

Phenocryst and microphenocryst: Augite and plagioclase constitute the phenocryst and microphenocryst of the D-1 basalt. They are fresh. Phenocrysts are distinguished from microphenocrysts by grain size, texture and chemical composition (Fig. VII-6). The apparent geometric mean diameter of phenocryst is more than 0.1 mm while that of microphenocryst is less than 0.1 mm. The modal composition of basalt is shown in Table VII-2.

Phenocryst augite is short prismatic, 0.2–0.5 mm in diameter. It composes 0.2–0.6 vol. % of the rock. Microphenocryst augite is granular, often forming crystal aggregates, and is 0.02–0.05 mm across. It even occurs in the chilled margin glass, suggesting that microphenocryst augite crystallized before eruption and quenching the magma on the seafloor. Augite shows undulatory extinction. The abundance of plagioclase phenocryst and microphenocryst ranges from 7 to 15 vol.%, and tends to increase from the rim to the interior of the pillow. Plagioclase phenocryst is thick tabular and is 0.3 to 1 mm in diameter. Glomerophyric aggregate of plagioclase is not uncommon. Plagioclase phenocryst shows normal zoning at the rim. It may show reverse zoning in the core (Fig. VII-8, PL-12). Plagioclase microphenocryst is thin tabular to hollowed or fork-shaped skeletal. Weak normal zoning may be observed at the rim.

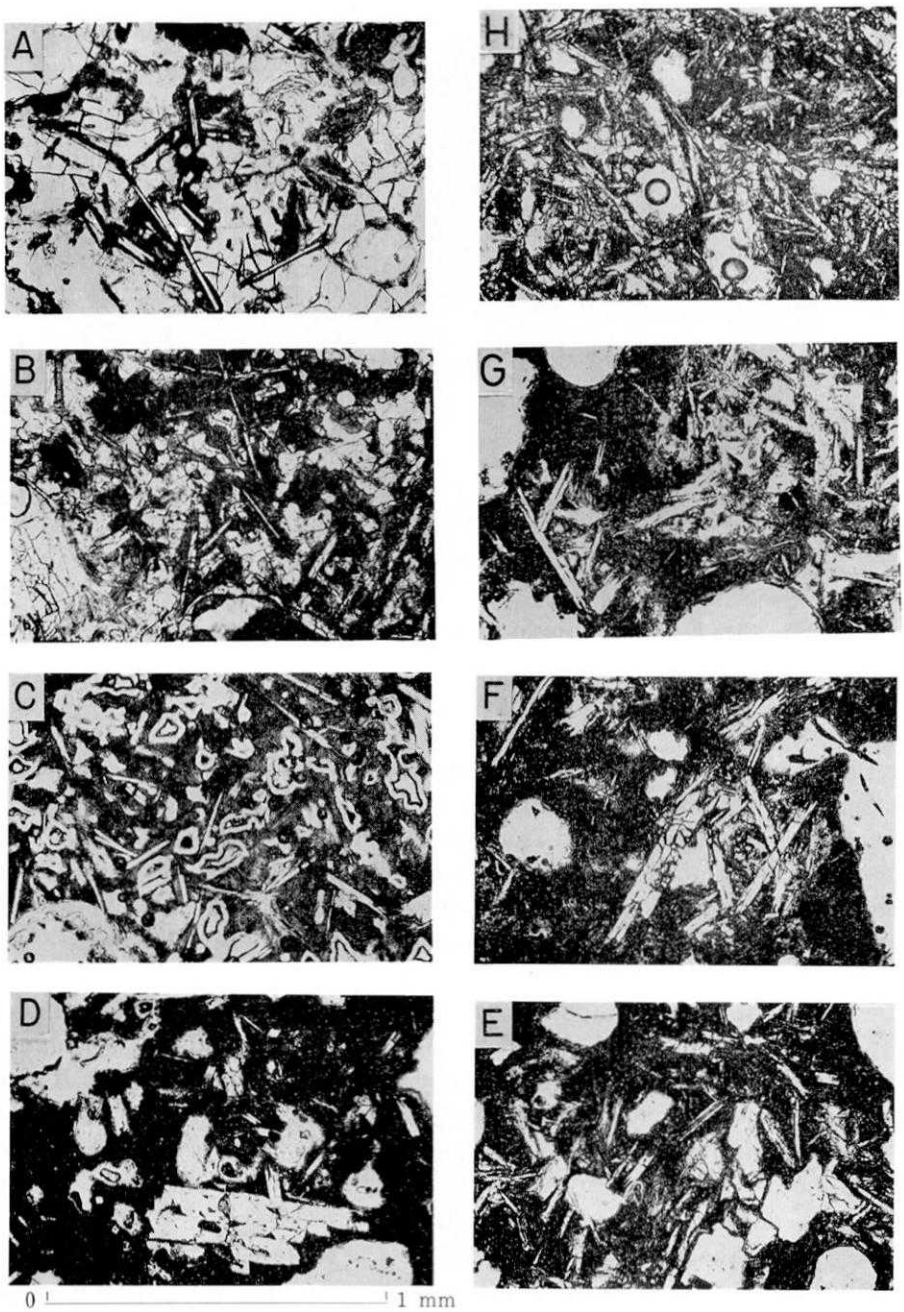

Fig. VII-6. Photomicrograph of D-1 basalt. Scale bar is 1 mm. A and B; Sideromelane glass zone, C, D, E and F; Tachylyte zone, G and H; Intersertal zone.

Table VII-2. Modal composition of DELP-85 D-1 basalt, analysed by H. SATO. Each column represents 2000 point counting in thin section. ph; Phenocryst, mph; Microphenocryst.

Distance from the periphery of a pillow		0-3 cm	3-6 cm	6-9 cm
augite	ph	0.5	0.6	0.2
	mph	0.8	1.8	1.9
plagioclases	ph	3.6	6.4	7.3
	mph	3.6	5.3	7.6
groundmass	fresh	71.7	85.6	75.0
	altered	19.8	0.4	8.0
vesicle	void	22.7	22.6	23.3
	clay fillings	12.0	6.0	6.5
crack filled by clay		0.1	n.d.	n.d.

* ph; Phenocryst, mph; Microphenocryst. Each column represents 2000 point counting in thin section.

Groundmass: The groundmass shows gradual textural variation and can be divided into three zones. They are from the margin to the interior of the pillow; A: chilled margin sideromelane zone, B: tachylyte zone, C: intersertal zone. Figure VII-6 illustrates the textural variation of the groundmass of D-1 basalt.

The groundmass of the sideromelane zone consists mostly of clear pale brown glass with a subordinate amount of devitrified glass around crystals (Fig. VII-6, A). The glass is partly altered to palagonite and smectite. Vesicles are round to subround and is 0.1 to 1 mm in diameter. Vesicles are partly filled (or lined) by smectite and hydro-iron oxide. The sideromelane zone is about 10 mm thick. The tachylyte zone extends from 10 to 35 mm from the periphery of the pillow. It is composed of crystallites of variolitic pyroxene and plagioclase, and is charged with minute granules of iron oxide. The grain size of the groundmass crystals is less than a few microns thick. This zone is suffered the least from alteration. Vesicles are irregular in form and are 0.05 to 1 mm in length. They are partly filled (or lined) by smectite and hydro-iron oxide. The intersertal zone occupies the interior part of the pillow and is distinguished from the tachylyte zone by the presence of microcrystalline plagioclase lath. Variolitic or interlocking plagioclase and augite compose the groundmass, with interstitial tachylyte charged with abundant granules of iron oxide. Plagioclase is commonly hollowed or fork-shaped skeletal, while augite is dendritic. Grain sized plagioclase and augite increases from less than 10 μm thick to 10-30 μm thick, while the amount of tachylyte

decreases toward the interior of the pillow. Vesicles are irregular and are 0.1 to 3 mm across. They are distributed zonally parallel to the margin of the pillow. Vesicles are partly infiltrated by tachylyte glass (segregation vesicles). They are also filled by hydro-iron oxide and smectite.

5. Phase chemistry

Chemical analysis of minerals and glasses were performed with Hitachi XMA-5A electron-probe microanalyzer of the Department of Earth Sciences, Kanazawa University (Table VII-3).

(1) Augite

Augite is the only pyroxene in the D-1 basalt. Mg/(Mg+Fe) ratio of augite ranges from 0.85 to 0.76, while the Wo content ranges from 45 to 34 (Fig. VII-7). Slight normal zoning is detected; i.e., Mg/(Mg+Fe) ratio of the core of augite ranges from 0.85 to 0.81, while that on the

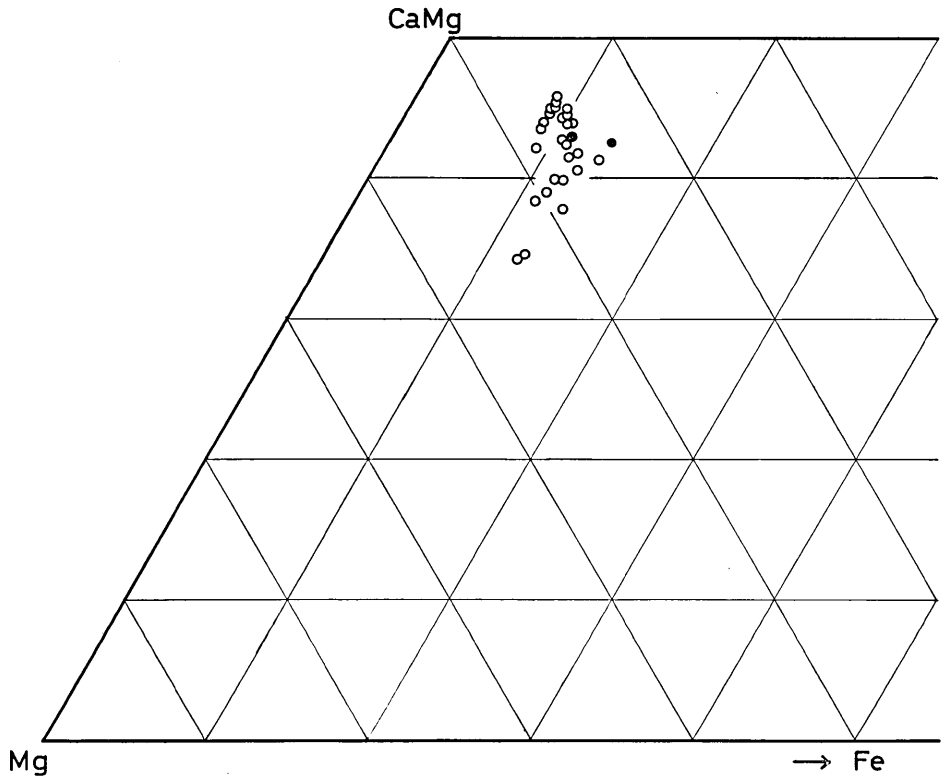

Fig. VII-7. Pyroxene quadrilateral of D-1 basalt. Empty circle; Phenocryst, Solid circle; Groundmass.

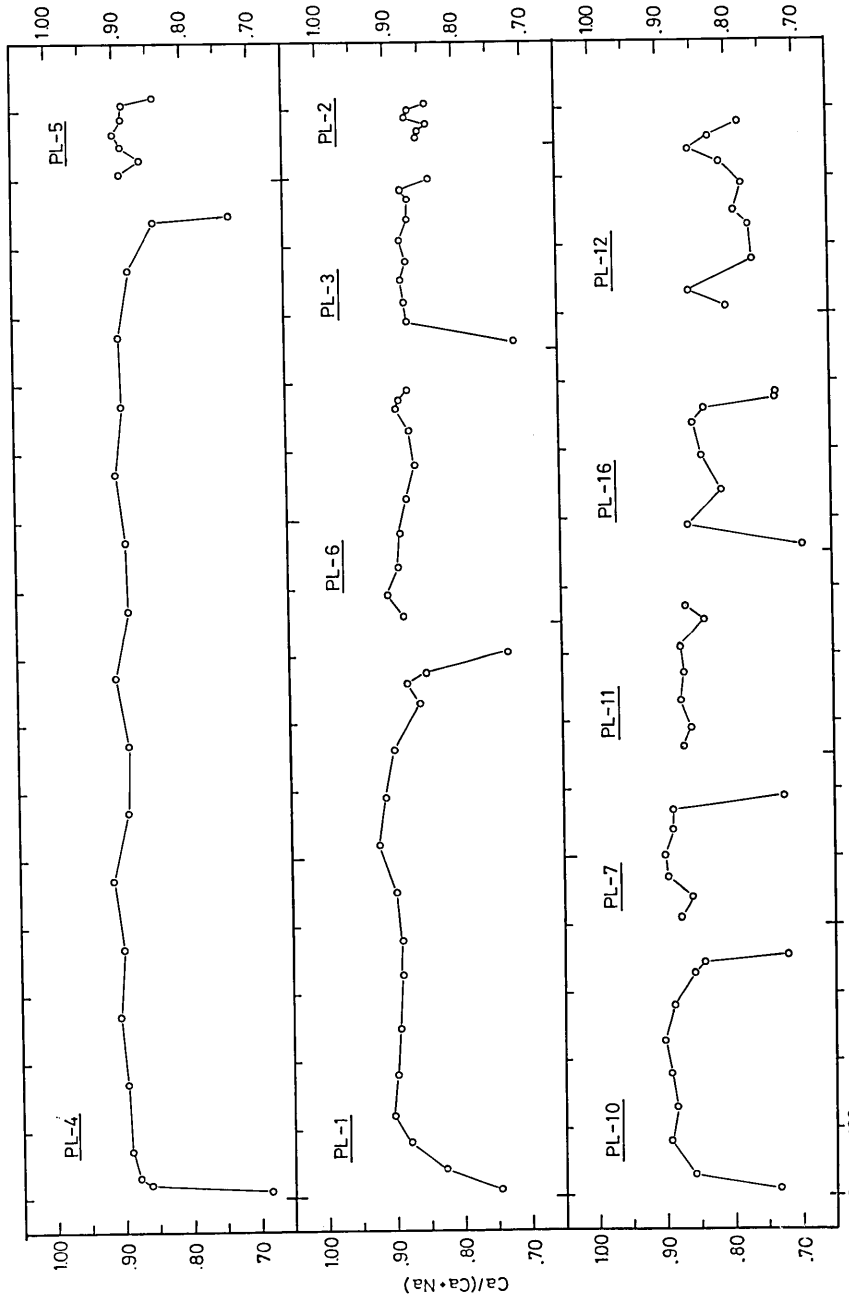

Fig. VII-8. Compositional profiles of plagioclase phenocrysts of D-1 basalt.

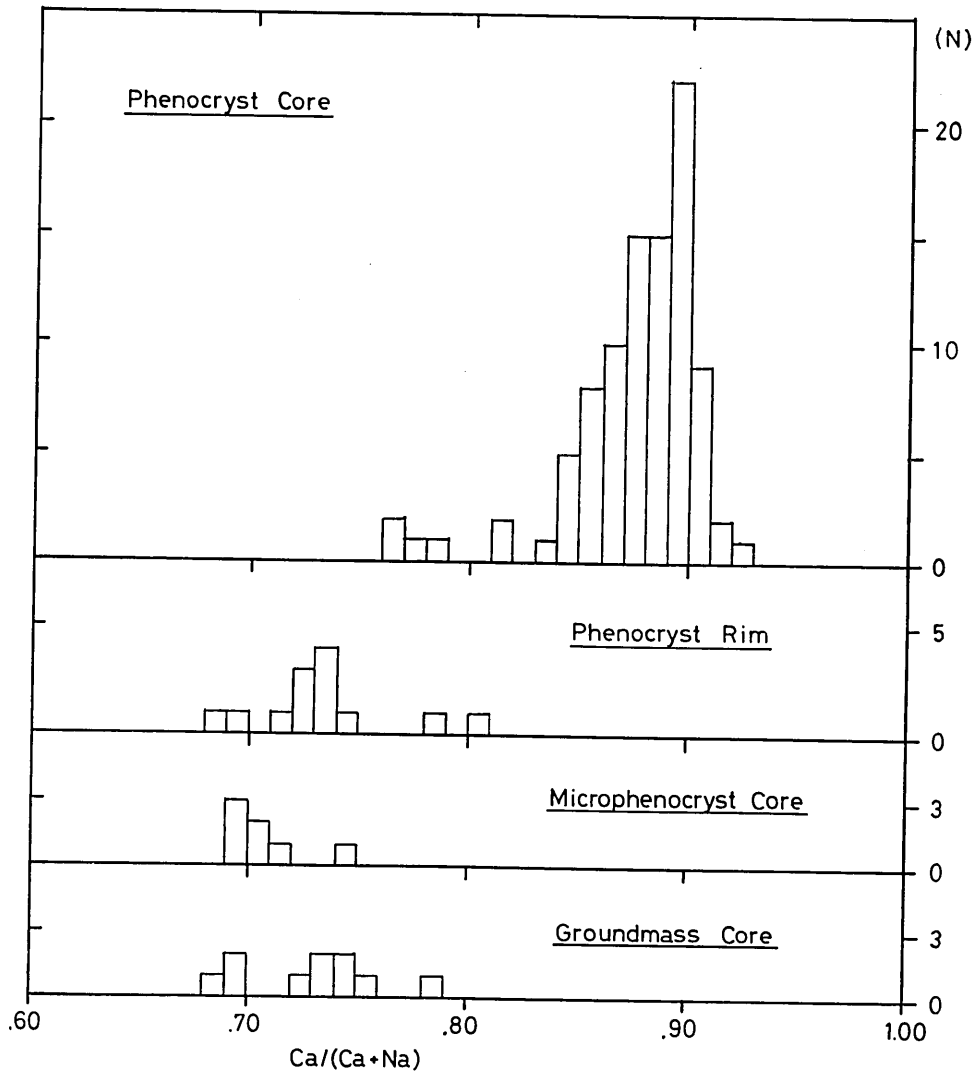

Fig. VII-9. Frequency of Ca/(Ca+Na) ratio of plagioclase phenocryst in D-1 basalt. Each box represents one analysis.

rim is 0.79–0.82. Mg/(Mg+Fe) ratio of the groundmass augite is 0.76–0.81. Al_2O_3 content of augite is 3–5 wt %. These chemical characteristics are common to augites in tholeiitic basalt of back-arc basins (*e.g.* HAWKINS and MELCIOR, 1985).

(2) Plagioclase

Compositional profiles of 11 plagioclase phenocrysts are shown in Fig.

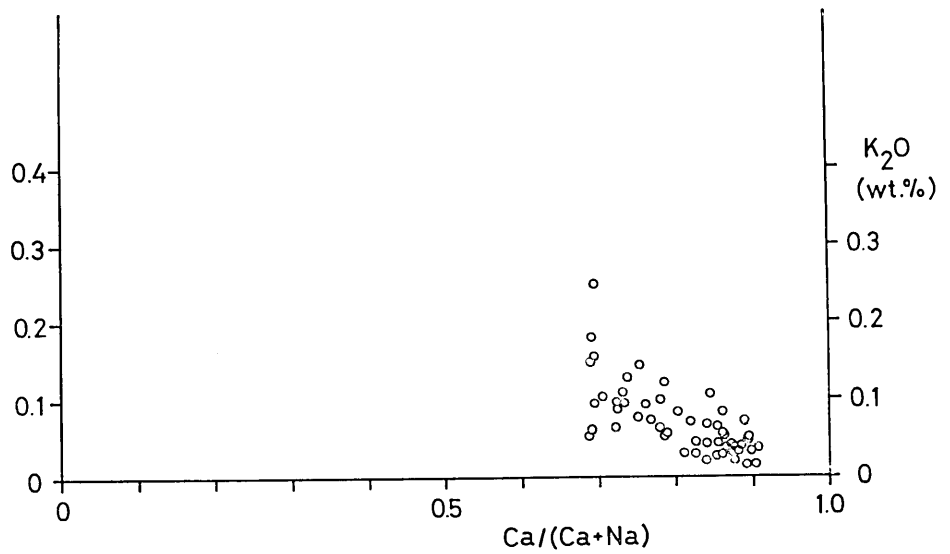

Fig. VII-10. K_2O versus Ca/(Ca+Na) relation of plagioclase in D-1 basalt.

VII-8. Most of the plagioclase phenocrysts in D-1 basalt have homogeneous cores (Ca/(Ca+Na)=0.92-0.85) with gradual normal zoning at the rim. Only two phenocrysts out of eleven showed reverse zoning within the core (grain #12 and #16, Fig. VII-8). The Ca/(Ca+Na) ratio of the inner core of the reversely zoned plagioclase is 0.81-0.76. The Ca/(Ca+Na) ratio of the rim of the plagioclase phenocryst ranges from 0.80 to 0.68, and is similar to those cores of microphenocryst and groundmass plagioclase (Fig. VII-9). The calcic nature of the core of plagioclase phenocryst may either be because of the plagioclase represents xenocryst precipitated from more primitive magmas before mixing and eruption of magmas (*e.g.*, DUNGAN *et al.*, 1978), or because the partition coefficient of Ca-Na between plagioclase and magma was under high water pressure during the intratelluric stage of crystallization. The K_2O content of plagioclase increases as the Ca/(Ca+Na) ratio decreases (Fig. VII-10), and it is generally below 0.15 wt %. The low K_2O content of the plagioclase is consistent with the low K/Na ratio of the host glass (Table VII-3).

(3) Glass

The electron-microprobe analyses of sideromelane and tachylyte glasses are shown in Table VII-3. They are basaltic and have the characteristics of back-arc basin basalts. The tachylyte glass is slightly richer in SiO_2 and Na_2O, and poorer in TiO_2 and K_2O than the sideromelane glass. The low total for the analyses of the sideromelane glass may be due to its high volatile content. The sideromelane glass is slightly quartz normative and has a FeO*/MgO ratio of 1.59-1.63. These chemical features are typical

Table VII-3. Phase chemistry of DELP-85 D-1 basalt, analysed by H. SATO. GL-1 is divitrified glass and GL-2, -3 and -4 are clear glass representing three analytical spots within the thin section.

SPOT*	GL-1	GL-2	GL-3	GL-4		CPX-1A	CPX-1B	PL-1A
phase	tachy-lyte	sidero-melane	sidero-melane	sidero-melane		augite	augite	plagio-clase
SiO_2	53.09	51.34	51.46	51.13	SiO_2	50.09	51.65	46.78
TiO_2	1.20	1.36	1.30	1.27	TiO_2	0.75	0.52	0.00
Al_2O_3	15.07	14.97	15.00	15.15	Al_2O_3	4.72	3.32	33.86
FeO	9.95	10.07	10.40	9.91	FeO	6.21	5.32	0.56
MnO	0.21	0.14	0.19	0.18	MnO	0.13	0.14	0.00
MgO	6.14	6.16	6.39	6.22	MgO	15.55	15.78	0.16
CaO	10.53	10.42	10.23	10.59	CaO	20.74	22.05	17.41
Na_2O	3.09	2.80	2.73	2.66	Na_2O	0.24	0.23	1.43
K_2O	0.42	0.47	0.43	0.48	K_2O	0.01	0.04	0.05
total	99.69	97.73	98.13	97.59	total	98.45	99.03	100.24
					(O=)	6.000	6.000	8.000
qz	2.4	2.2	2.3	2.2	Si	1.871	1.914	2.149
or	2.5	2.8	2.6	2.9	Al	0.208	0.145	1.833
ab	26.2	24.2	23.5	23.0	Ti	0.021	0.015	0.000
an	26.0	27.5	27.9	28.6	Fe	0.194	0.165	0.022
wo	11.0	10.0	9.9	10.5	Mn	0.004	0.004	0.000
en	15.3	15.7	16.2	15.8	Mg	0.866	0.872	0.857
fs	11.2	11.2	11.8	11.2	Ca	0.830	0.875	0.857
mt*	3.2	3.3	3.4	3.3	Na	0.017	0.017	0.127
il	2.3	2.6	2.5	2.5	K	0.001	0.002	0.003
					total	4.013	4.008	5.000
(mol %)								
Ol	15.2	16.0	17.3	16.2	Mg	.458	.456	
Cpx	20.1	19.5	17.8	19.2	Ca	.439	.458	
Qz	23.5	23.7	25.2	24.0	Fe	.103	.086	
Pl	41.2	40.8	39.7	40.5				
* Fe(3)/(Fe(3)+Fe(2)) was assumed to be 0.2 in calculating C.I.P.W. NORM.					Mg/(Mg+Fe)	.817	.841	
					Ca/(Ca+Na)			.871

of evolved ocean ridge and back-arc basin basalts. Fig. VII-11 compares TiO_2 and K_2O with Feo*/MgO of D-1 basalt and basalts from other back-arc basins, N-type MORB and island arc tholeiites. The TiO_2 content of D-1 basalt is high and may distinguish it from island arc tholeiites. Whereas the K_2O content of D-1 basalt is distinctly higher than N-type MORB, it falls within the compositional range of back-arc basin basalt. The phase chemistry as well as the petrography of D-1 pillow basalt suggest that it was formed in a back-arc basin.

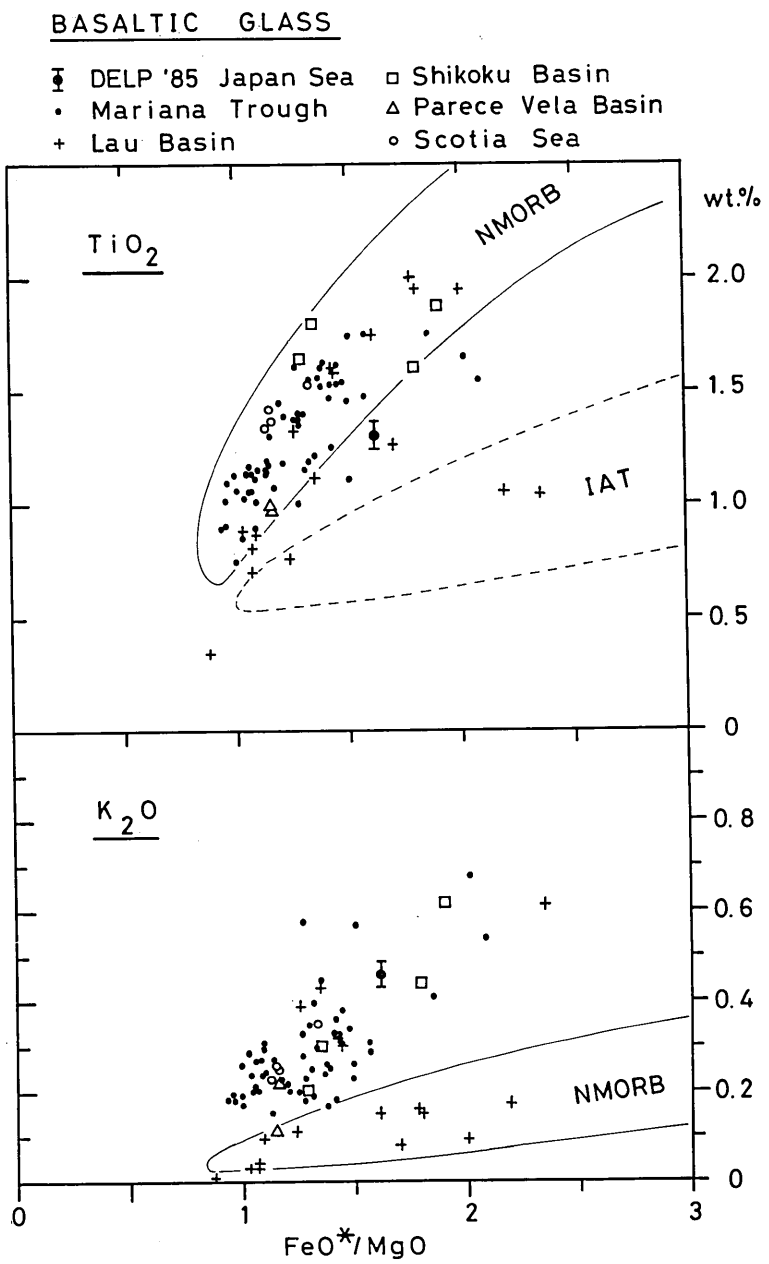

Fig. VII-11. TiO_2 and K_2O versus FeO*/MgO relation of basaltic glass of D-1 basalt of other back-arc basins (FRYER *et al.*, 1982; HAWKINS and MELCIOR, 1985), N-type MORB and island-arc tholeiite.

6. Petrochemistry

The bulk chemical contents of the major and minor elements of the tachylyte and intersertal zones of D-1 basalt were analyzed by X-ray fluorescence analysis (XRF) and instrumental neutron activation analysis (IRAA) methods, respectively. Major element abundances in glasses of tachylyte and sideromelane zones were analyzed by electron microprobe. The XRF analysis was performed using Rigaku system 3080 at the Industrial Research Institute of Hyogo Prefecture and the IRAA analysis using the Kyoto University Reactor. The analytical results are presented in Tables VII-3 (GL-1-GL-4) and VII-4.

Chemical characters of D-1 basalt imply that D-1 basalt has aspects similar to those reported on the marginal basin basalts (MBB). (1) SiO_2 contents are 50.50 to 53.08 in weight %. The amounts of total Fe as FeO are 9.55 to 10.70% and more abundant than those of calc-alkaline basalts. MgO contents are 5.46 to 6.39% and less than primitive calc-alkaline and island arc tholeiitic basalts. (2) D-1 is more abundant in TiO_2 (1.20 to 1.36%) than island arc tholeiitic and calc-alkaline basalts. The abundance is similar to those of N-type MORB and MBB from the Shikoku Basin, the Mariana Trough and the Lau Basin. (3) D-1 basalt is more abundant in alkali elements than N-MORB, and the amounts are similar to those of

Table VII-4. Bulk major and trace element analyses of the basalt dredged at the D-1 site in the Yamato Basin, analysed by T. MATSUDA.

Bulk major element				Trace element	
SiO_2	50.50	qz	2.4	Rb	9.0
TiO_2	1.24	or	3.3	Ba	27.2
Al_2O_3	15.86	ab	19.4	Co	35.1
Fe_2O_3*	11.89	an	31.4	Cr	122
MnO	0.12	di		Cs	1.1
MgO	5.46	wo	9.5	Hf	0.12
CaO	11.49	en	4.6	Sc	43.4
Na_2O	2.31	fs	4.6	Ta	0.04
K_2O	0.54	hy		Th	0.61
P_2O_5	0.38	en	8.9	U	1.10
Total	99.79	fs	8.8	La	7.27
		mt	2.5	Ce	14.4
		il	2.4	Sm	2.72
		ap	1.0	Eu	1.04
				Tb	0.68
				Yb	2.11
				Lu	0.31

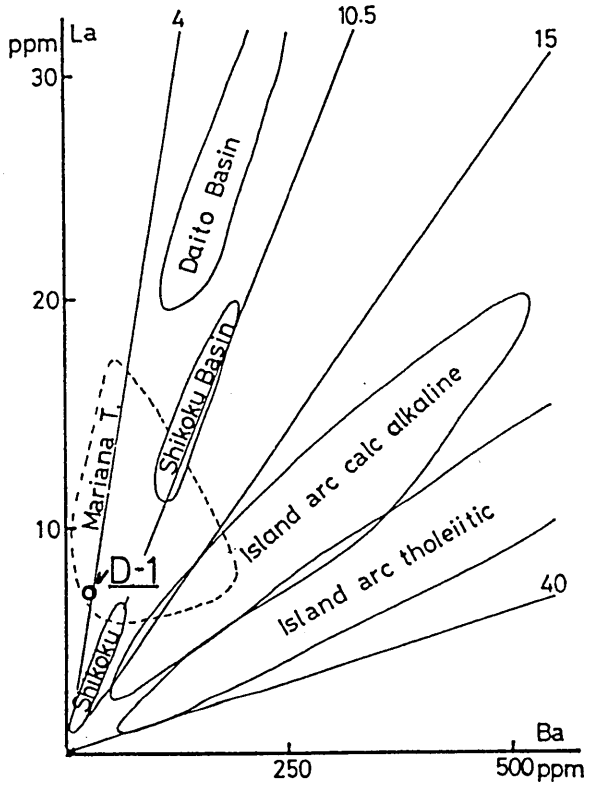

Fig. VII-12. Ba/La ratio of D-1 basalt.

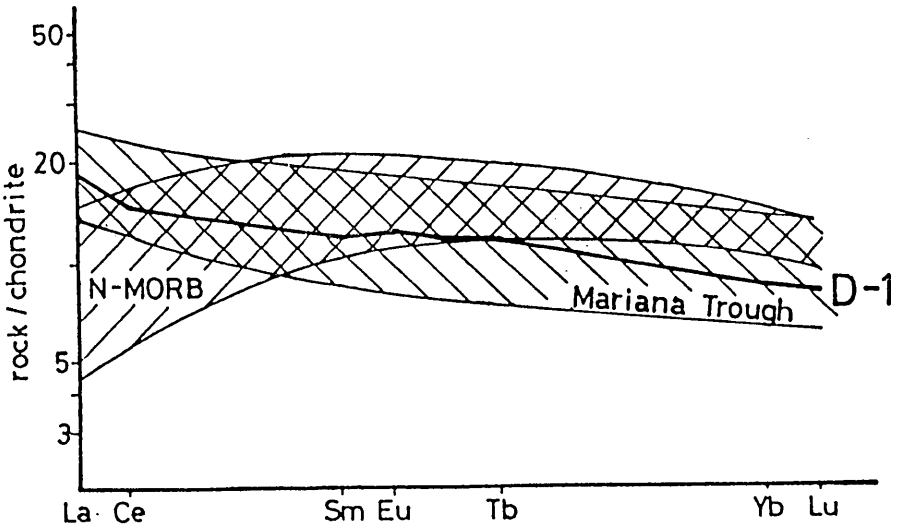

Fig. VII-13. Chondrite normalized pattern of rare-earth elements of D-1 basalt.

MBB. (4) Ba/La ratio (=3.7) of D-1 basalt is similar to those of N-MORB and MBB (Fig. VII-12) and is distinctly lower than island arc basalts. (5) Chondrite normarized abundances of rare-earth elements shows almost a flat pattern but light rare-earth elements are slightly enriched (Fig. VII-13). The pattern shows good agreement with those of MBB but not with those of N-type-MORB which are depleted in light rare-earth elements.

These chemical features imply that D-1 basalt resembles tholeiitic basalts from marginal basins such as the Shikoku Basin, Mariana Trough and Lau Basin which have been thought to have originated during the formation of the basalt. D-1 basalt is the first tholeiitic sample obtained from the basins of the Japan Sea.

7. K-Ar age of a basalt dredged at the D-1 site in the Yamato Basin

K-Ar age was determined for the basaltic rock dredged at the D-1 site in the Yamato Basin. The dated sample was a basaltic pillow lava block of about 400 g with chilled margins. The block was cut into five slabs. Among them, the slab D (D-1, No. 1-D) was used for K-Ar dating. A central portion from the slab D, which is relatively fresh and contains no chilled margin, was cut out for analysis. Even this portion is, however, not completely fresh and a part of its groundmass has the possibility of alteration to some extent. To remove the impurities in vesicles and cracks, the sample was boiled in distilled water before analysis.

The amount of radiogenic ^{40}Ar was determined by the isotope dilution method with ^{38}Ar as a tracer. A Reynoldstype mass spectrometer was used for Ar analysis in a similar manner to that reported before (KANEOKA *et al.*, 1980). The value of K content obtained by the EPMA (Table VII-3) was used to calculate the K-Ar age.

The result is shown in Table VII-5. The apparent K-Ar age is about 7.3 Ma. Since the atmospheric contamination level in this sample is relatively large (about 81%), the analytical error becomes about 0.5 Ma. As mentioned before, this sample was not completely fresh. The glass content in this sample does not exeed 50% under a microscopic observation. Hence this sample probably contains no significant amount of excess ^{40}Ar, Thus the K-Ar age would indicate the minimum value for the eruption age of this sample.

We have obtained some K-Ar and ^{40}Ar-^{39}Ar ages for volcanic rocks dredged from the Yamato Seamount Chain in the broad sense. They show K-Ar ages of 6-13 Ma and ^{40}Ar-^{39}Ar ages of 10-17 Ma (KANEOKA *et al.*, 1986). These rocks are primarily alkali basalts and andesites TATSUMOTO *et al.*, 1986). Since they were not completely fresh, there is

Table VIII-5. K-Ar age of the basalt dredged at the D-1 site in the Yamato Basin, dated by I. KANEOKA.

Sample No.	Rock name	Weight (g)	$(^{40}Ar)_{rad.}$ ($\times 10^{-8}$ cm^{3}STP/g)	$\frac{(^{40}Ar)_{air}}{(^{40}Ar)_{tot.}}$ (%)	K (%)	Age (Ma)
D-1, No. 1-D	Tholeiitic basalt	2.231	12.79	80.6	0.448	7.34±0.51

N.B.

K-Ar age was calculated by using following values (STEIGER and JÄGER, 1977).

$\lambda_e = 0.581 \times 10^{-10}$ yr^{-1},

$\lambda_\beta = 4.962 \times 10^{-10}$ yr^{-1},

$\frac{^{40}K}{K} = 1.167 \times 10^{-4}$ moles/mole.

The uncertainty in the age indicates one standard deviation.

a possibility that at least some of them might have lost radiogenic ^{40}Ar due to alteration. Furthermore ^{40}Ar-^{39}Ar ages seem to show systematically older values than those of K-Ar ages. Taking these into account, it is inferred that the Yamato Seamount Chain might have been formed 10–20 Ma. However we cannot decide whether these seamounts were formed at the same period or not based upon the absolute age determination method only.

Although we cannot conclude at present whether the present sample (D-1, No. 1-D) was formed at the same period as those of the Yamato Seamount Chain, we can at least say that it was probably formed at a time which was not so different from them.

8. Geostructure

8-1. Acoustic discontinuities

Relatively distinct two acoustic discontinuities were observed in seismic reflection records. Those are shown by characteristic reflectors "I" and "II" (Figs. VII-14 and VII-15), suggesting marked tectonic movement during the formation of the reflectors. Reflector II is at a top of the acoustic basement and reflector I exists within sediments above reflector II. Reflector I may have been formed during the Pliocene Epoch and reflector II in the Late Miocene Epoch inferred from the stratigraphic correlation between seismic reflection and drilling data (KARIG *et al.*, 1975; ISHIWADA and HONZA, 1984; TOKUYAMA *et al.*, 1987 (part III of this report)). All the sedimentary layers covering reflector II are well continuous in the study area although those were slightly dislocated by faults. Thus our data showed that large tectonic events such as ocean floor spreading did not occur during and after deposition of sediments covering reflector II.

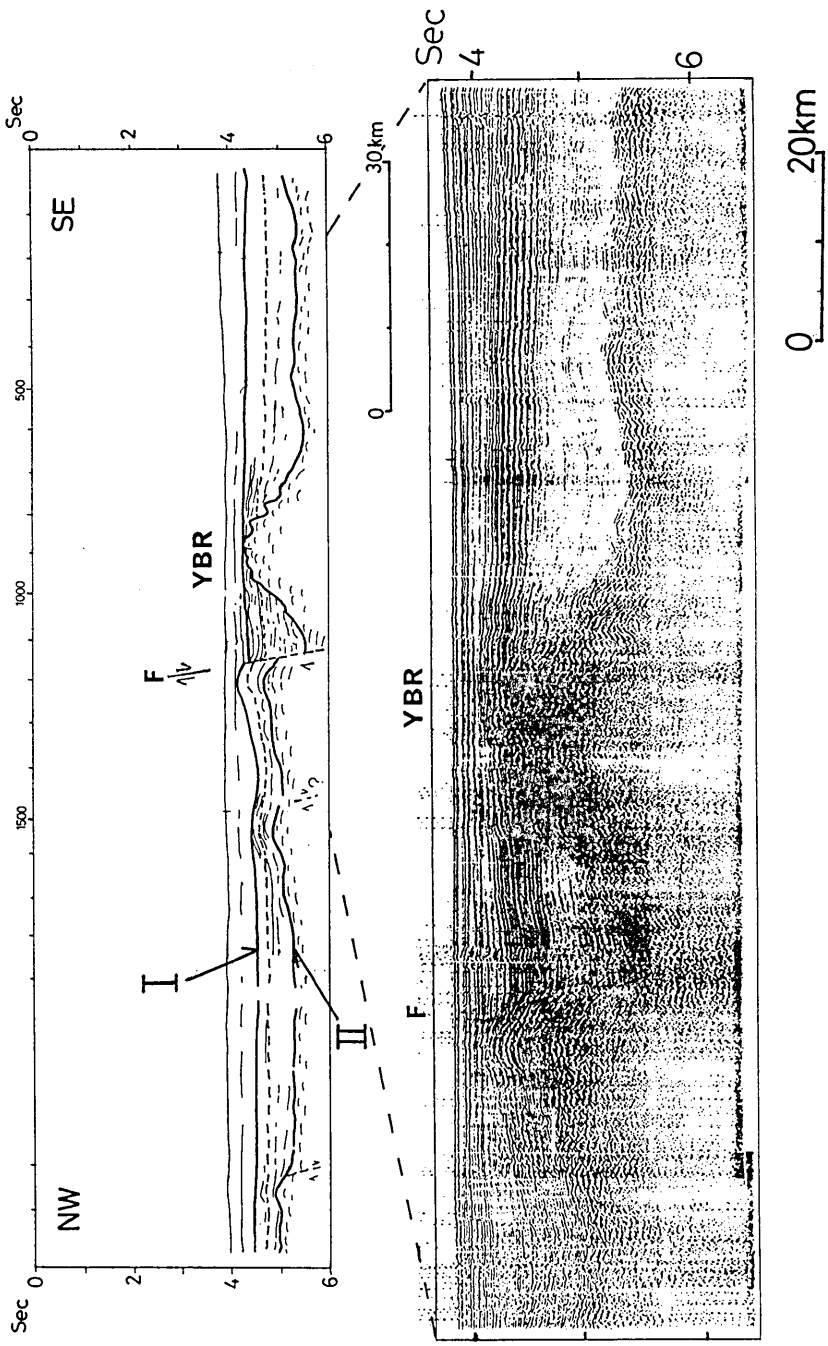

Fig. VII-14. Seismic reflection profile in Line 4 (single channel profiling record) showing stratigraphic relation in the southern part of the Yamato Basin. Location is shown in Fig. VII-1. Two way travel time is represented by "Sec". Reflectors "I" and "II" are explained in the text. Bottom figure represents P-4 in Fig. VII-1. YBR; Yamato Basin Ridge, F; Fault.

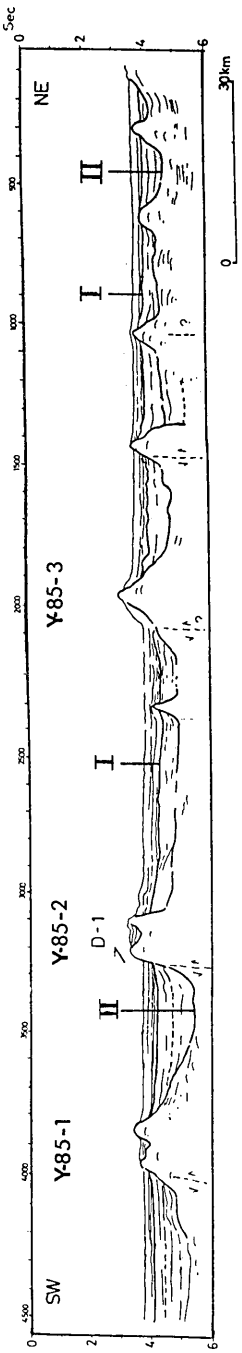

Fig. VII-15(A).

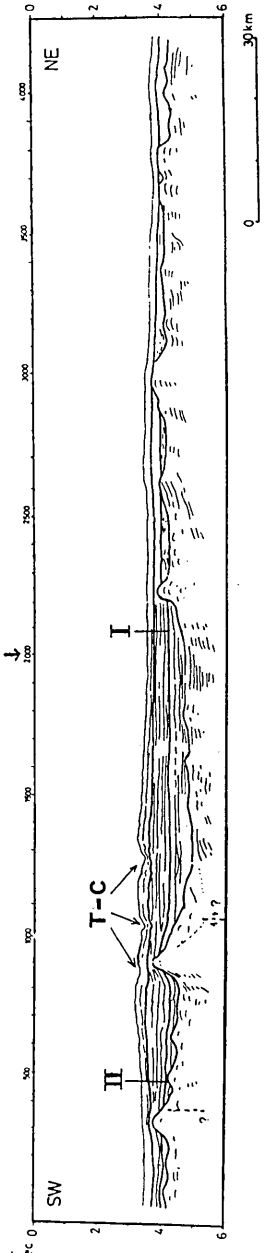

Fig. VII-15(B).

Fig. VII-15. Interpreted multi-channel profiling records. Locations are shown in Fig. VII-1. Reflectors "I" and "II" are explained in the text.

Fig. VII-15(A). Line 1. Y-85-1, -85-2 and -85-3 represent the Yamato-85-1, -85-2 and -85-3 Knolls.

Fig. VII-15(B). Lines 2 and 3. T-C; Toyama Deep Sea Channel.

8-2. Central ridge of the Yamato Basin

Seismic reflection data revealed a feature of the central ridge buried by a sedimentary cover of thickness from 0 to 1000 m (Figs. VII-3, VII-14 and VII-15). Location of the ridge was plotted on the map based upon our data and that from the GEOLOGICAL SURVEY OF JAPAN (1979), HILDE and WAGEMAN (1973) and LUDWIG *et al.* (1975) (Fig. VII-16). The ridge was tentatively named the Yamato Basin Ridge (YBR). The trend of the YBR can be traced through the Yamato-85-1, -85-2, -85-3, -85-4 Knolls, the Meiyo Seamount (Me; Fig. VII-2), Second Meiyo Seamount (Me-2) and Third Meiyo Seamount (Me-3). Fragments of pillow basalt from the Yamato-85-2 Knoll (D-1) were taken from the topographic peak of the ridge (Fig. VII-4(B)). The YBR is separated into six segments by transverse faults. The apparent K-Ar age of the basalt from the Yamato-85-2 Knoll is 7.3 ± 0.51 Ma (Late Miocene) (Table VII-5). On the other hand, 6-17 Ma (K-Ar and ^{40}Ar-^{39}Ar ages) was attained from the Meiyo and Second Meiyo Seamounts (KANEOKA *et al.*, 1986). Therefore, the ridge formation seems to have been progressed sometime during the Miocene Epoch.

Another series of seamounts and knolls lies subparallel to the YBR in the north, which is called the Yamato Seamount Chain in the narrow sense. The Yamato Seamount Chain also shows buried ridge feature judging from the data of DELP-85 cruise and other data. Ages of 7-15 Ma (^{40}Ar-^{39}Ar ages) were given from the Yamato Seamount (KANEOKA *et al.*, 1986). The Yamato Seamount Chain might also have been formed sometime in the Miocene Epoch.

8-3. Faults

Two directions of fault systems were determined (Fig. VII-16). One is a system trending NE-SW subparallel to the YBR. The cross section in Fig. VII-14 shows a fault (F) located northwest of the YBR. It is apparently a normal fault with the southeast side down. The fault seems to cut all the layers below reflector I. The sedimentary cover above the reflector I, however, is not suffered from the fault deformation. The fault had to be active until the Late Pliocene Epoch. This type of fault forms a boundary on the southeastern wall of the ridge of the Yamato Seamount Chain.

Another system of faults is a group of transverse faults offsetting the axis of the YBR into 6 segments. The 3.5 KHz and multi-channel seismic reflection records show that there is a distinct difference in topographic level and depth of the acoustic basement between at the northern and southern sides of the Yamato-85-3 Knoll (Fig. VII-4(C)). The seafloor and acoustic basement are lower by about 200 m on the southern

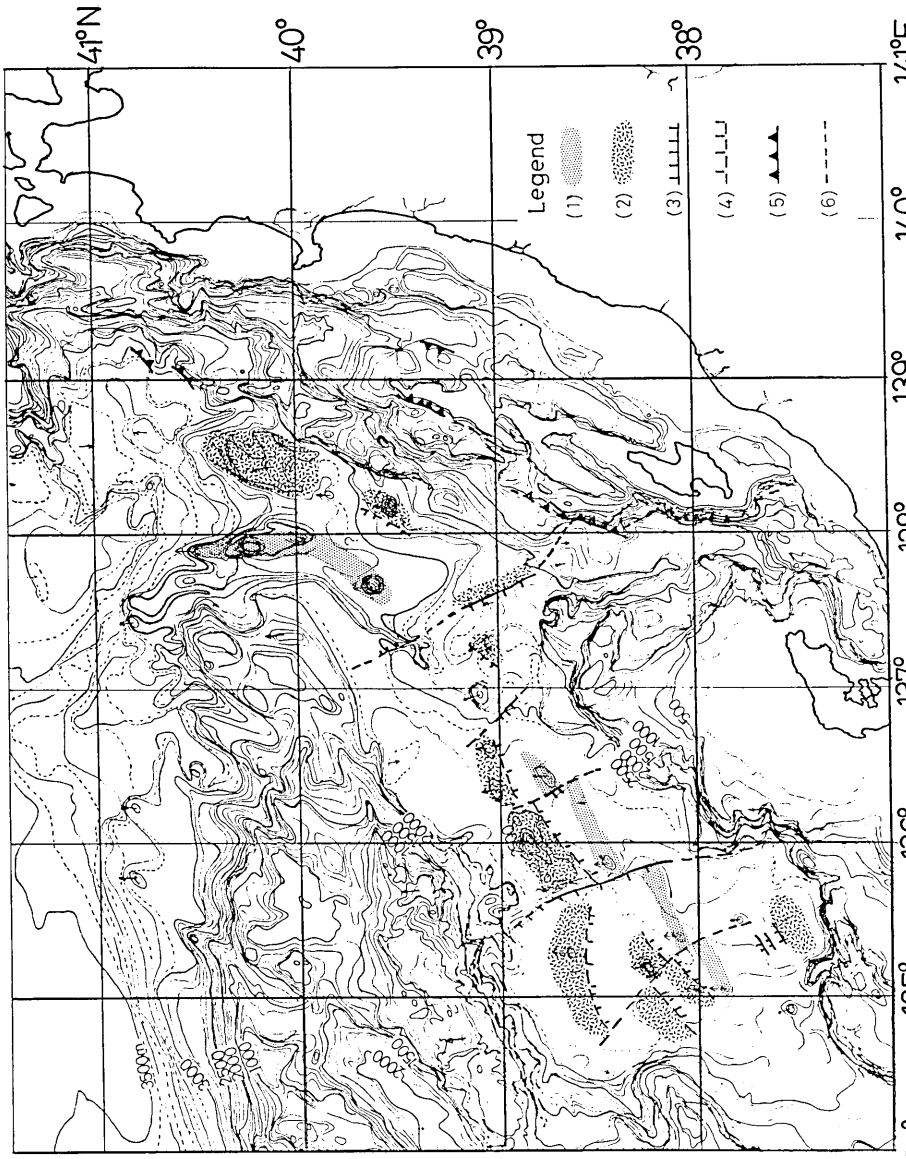

Fig. VII-16. Geostructural map, compiled from the present data and available data from various sources. Thrusts at the continental slope off the western coast of Sado Island were interpreted from LUDWIG *et al.* (1975) and GEOLOGICAL SURVEY OF JAPAN (1979). Legend: (1); YBR, (2); Yamato Seamount Chain in the narrow sense and basement highs, (3); Fault. Teeth show the down thrown side, (4); Buried fault, (5); Thrust. Teeth show the upthrown side, (6); Estimated fault.

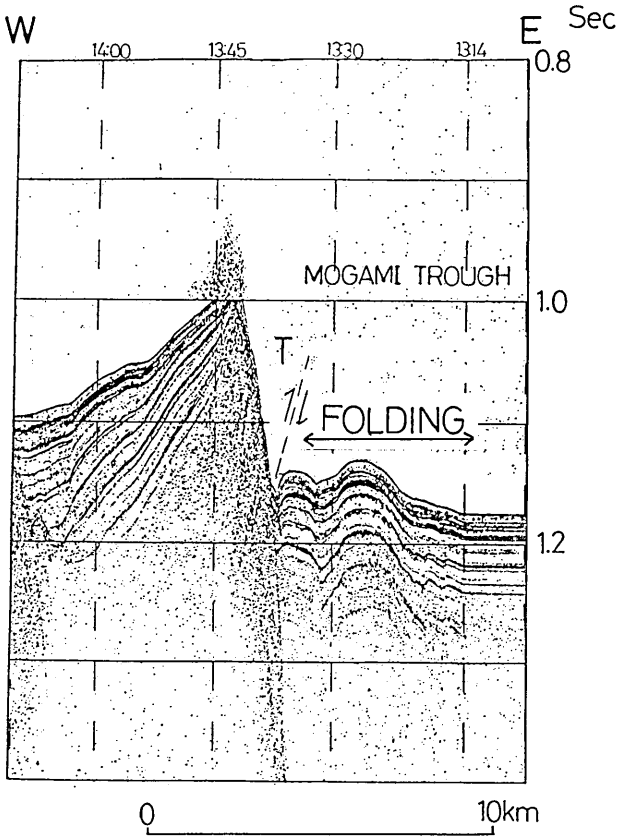

Fig. VII-17. P-9. Profile showing very new compressional features around the Mogami Trough represented by the 3.5 KHz subbottom profiling record. An estimated fault associated with folding represents a thrust (T). Location is shown in Fig. VII-1.

side. In addition to this, a feature showing a rift or graben was observed on the profiling record as shown in Fig. VII-4(C). The rift, a V-shaped depression, seems to dislocate Pliocene-Pleistocene sediments. These observations indicate that there exists a large fault on the southwestern foot of the Yamato-85-3 Knoll, with the SW side subsided. The same type of faults were recognized at the foot of the Yamato-85-2 and Yamato-85-4 Knolls (Figs. VII-4(B) and (D)).

Sediments on the reflector II is thicker on the southern side of the fault scarp associated with the Y-85-2 Knoll than on the northern side (Fig. VII-15(A)), and the reflector I is vertically distorted and dislocated by faults. This suggests that the vertical movement occurred during the deposition of sediments since the Late Miocene/Pliocene Epochs and that the vertical faulting movement again occurred after the formation of the

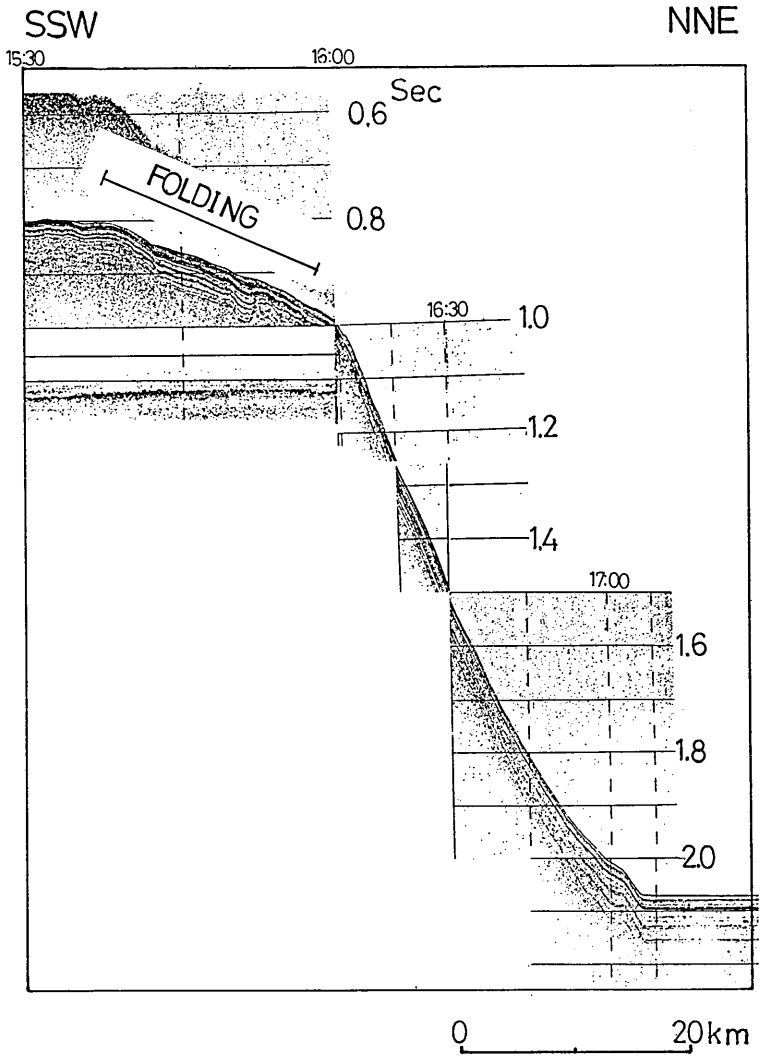

Fig. VII-18. Profiles showing very new folding structure in the continental slope off the NE Japan coast. Locations are shown in VII-1.
Fig. VII-18(A). P-10. Middle slope of the Mogami Trough.

reflector I. In addition, those faults seem to transversely offset the YBR (Fig. VII-16).

Very young faults were found on 3.5 KHz subbottom profiles as shown in Figs. VII-4(B), VII-4(D) and VII-4(E). Only the upper part of the younger sediments on the reflector I is slightly offset by normal faults. They are probably active and most are located at the southern foot of the knolls, such as the Yamato-85-2 Knoll, the Yamato-85-4 Knoll and

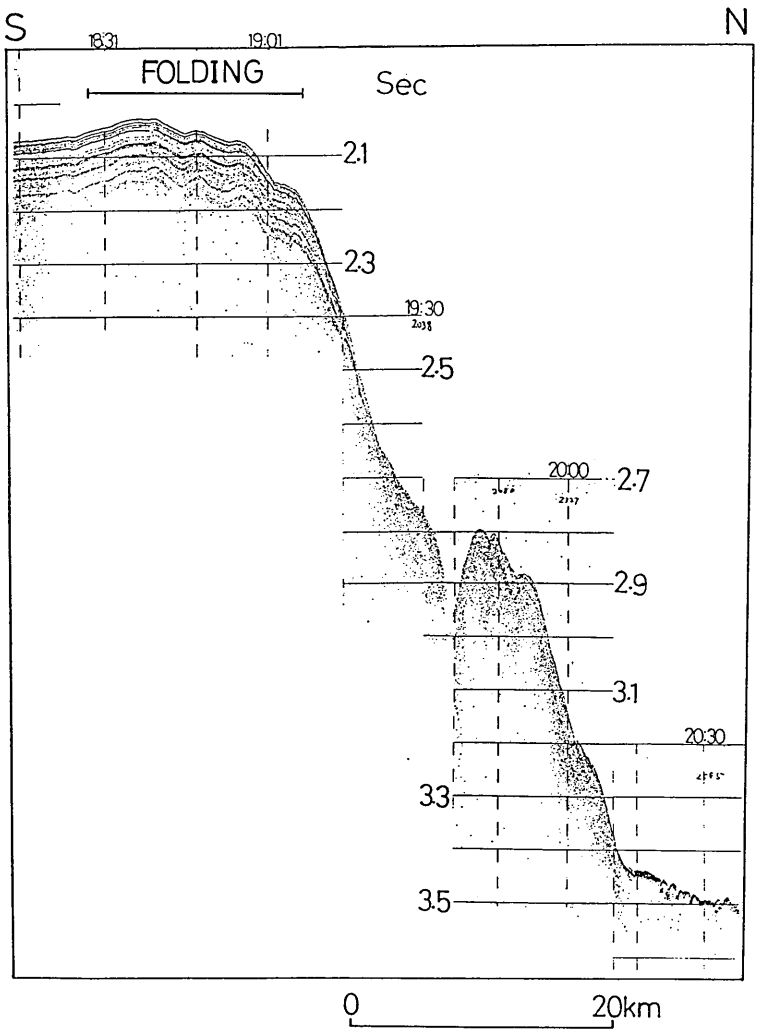

Fig. VII-18(B). P-11. Lower slope of the Mogami Trough.

Meiyo Seamount. The location of those young faults well coincides with the transverse big faults crossing the ridge. This shows that the vertical movement occurred in Late Pleistocene or more recent Epoch.

8-4. Compressional features on the continental slope off Northeast Japan

Fig. VII-17 shows a fault scarp accompanied by folding, trending from the NNE to the SSW. The scarp may have been formed by a thrust fault (T in Fig. VII-17), because the associated folds strongly show the effect of compressive stresses. Since the uppermost surface of the sedimentary layer is folded, this tectonism is recent and consistent with

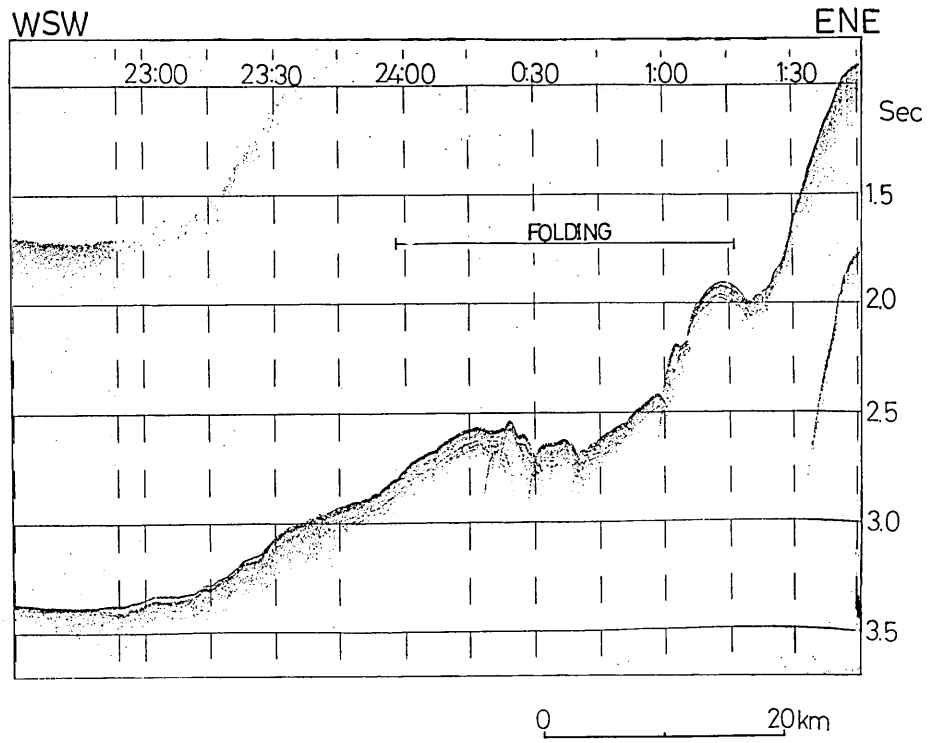

Fig. VII-18(C). P-8. Lowest slope (western side) of the Sado Ridge.

the present regional compressive stress field of Northeast Japan (NAKAMURA and UYEDA, 1980).

Fig. VII-18 (A, B and C) shows a very young, smaller scale folding structure concordant with topographic relief. The trend of folding axes is not clear, but this also may be related to the same very young compressional stress field as those in Northeast Japan. Fig. VII-19 (A and B) suggests that steep cliffs are fault scarps thrust up judging from the analogy of topographic features in Fig. VII-17 and from the existence of a visual thrust on the profile (T_1 in Fig. VII-19 (B)).

9. Tectonics and discussion

Seismic refraction survey carried out during the DELP-85 cruise in the central part of the Yamato Basin showed the crustal structure similar to that of a typical oceanic basin but with a comparatively large crustal thickness (HIRATA *et al.*, 1987 (part II of this report)). The isotopic studies of the seamount in the Yamato Basin, including basalt recovered from station D-1, indicate that these rocks were derived from a depleted

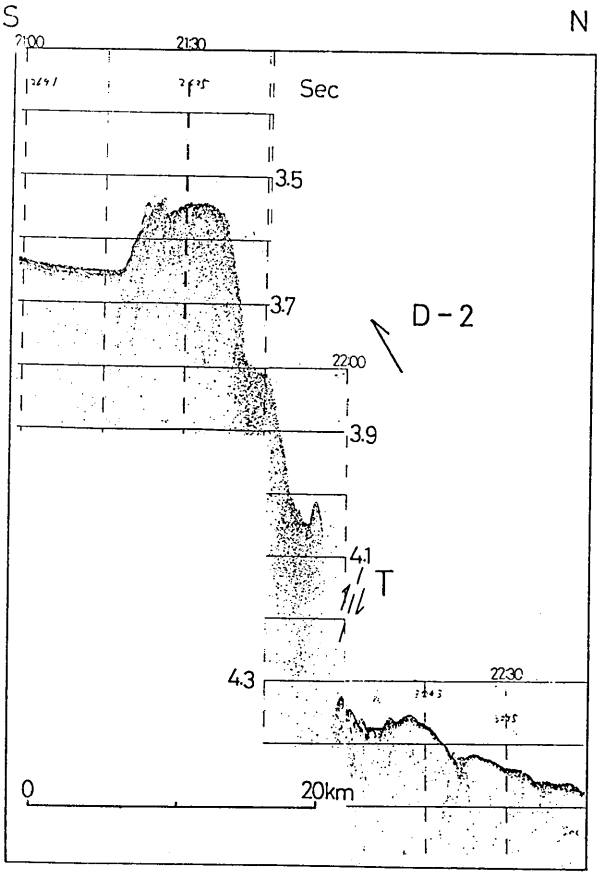

Fig. VII-19. Profiles showing the lowest scarp of the continental slope off Northeast Japan. Dredging stations D-2 and D-3 are represented. Locations are shown in Fig. VII-1.

Fig. VII-19(A). P-12. The northern terminal of the Sado Ridge. Dredge station D-2 is represented. T; Thrust estimated.

source, in contrast to the results for subaerial rocks which indicate derivation from a chondritic to enriched source (TATSUMOTO *et al.*, 1986). LUDWIG *et al.* (1975) stated that if spreading did occur, it must have occurred prior to the deposition of the apparent 3.5 km/sec layer above the basement and the younger sediments.

The YBR is located in the central part of the Yamato Basin (Fig. VII-20). Basalt dredged from the Yamato-85-2 Knoll located on the ridge is similar to MBB and gave a K-Ar age of 7.3 Ma. It supports the existence of the oceanic crust of the marginal sea type beneath the central part of the Yamato Basin by refraction studies (HIRATA *et al.*, 1987). The YBR may have been a spreading center in the Yamato basin

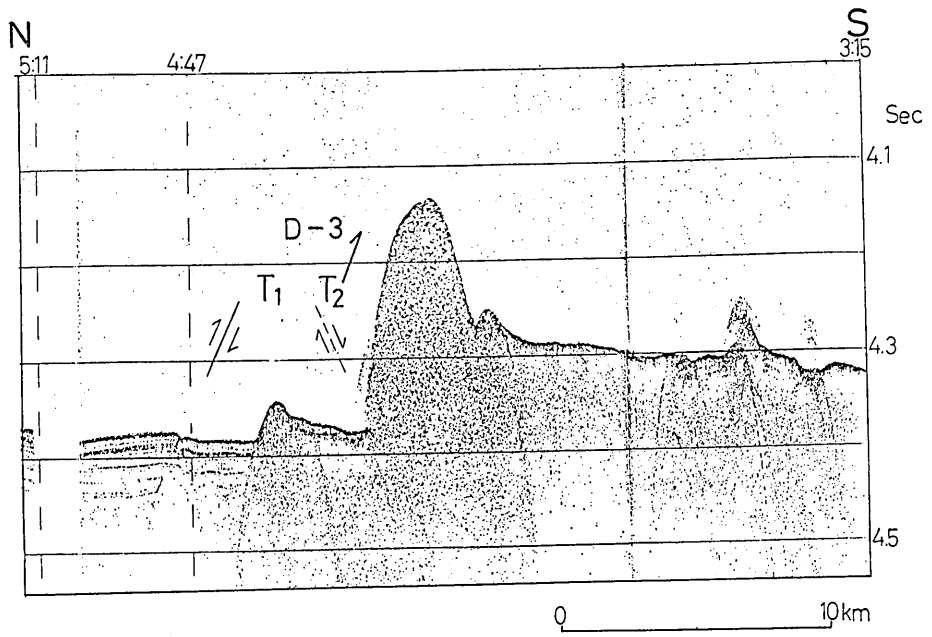

Fig. VII-19(B). P-13. The lowest scarp of the continental slope off the coast of Aomori Prefecture. T_1; Thrust observed, T_2; Thrust estimated.

in the Miocene Epoch. The ridge corresponds to the southern half of the "basement high" of LUDWIG *et al.* (1975) and seems to coincide with the fossil spreading center in the Yamato Basin suggested by HILDE and WAGEMAN (1973).

Radiometric ages of volcanoes of 6–15 Ma in the Yamato Basin suggest that volcanisms in the Yamato Basin had some relationship to the opening of the Japan Sea around 15 Ma (OTOFUJI *et al.*, 1986). If the Yamato Basin was formed as a part of spreading processes of the Japan Sea, our petrologic and sedimentological data suggest that the spreading of the basin occurred along the YBR before the Late Miocene Epoch and ceased during Late Miocene Epoch.

It is estimated that the Yamato Seamount Chain was also active sometime during Middle to Late Miocene Epoch judging from ages of 6–14 Ma at part of the chain (Fig. VII-20). Normal faults are distributed along the southeastern foot of the chain (F in Fig. VII-14). The Northwestern slope of the Yamato Seamount Chain is tilted against the YBR, showing that the Yamato Seamount Chain is the tilted margin of the YBR. Taking this into account, the formation of the YBR is thought to have been younger than the Yamato Seamount Chain.

There exist transverse faults which form offsets of the YBR. This feature could be formed by horizontal as well as vertical differential

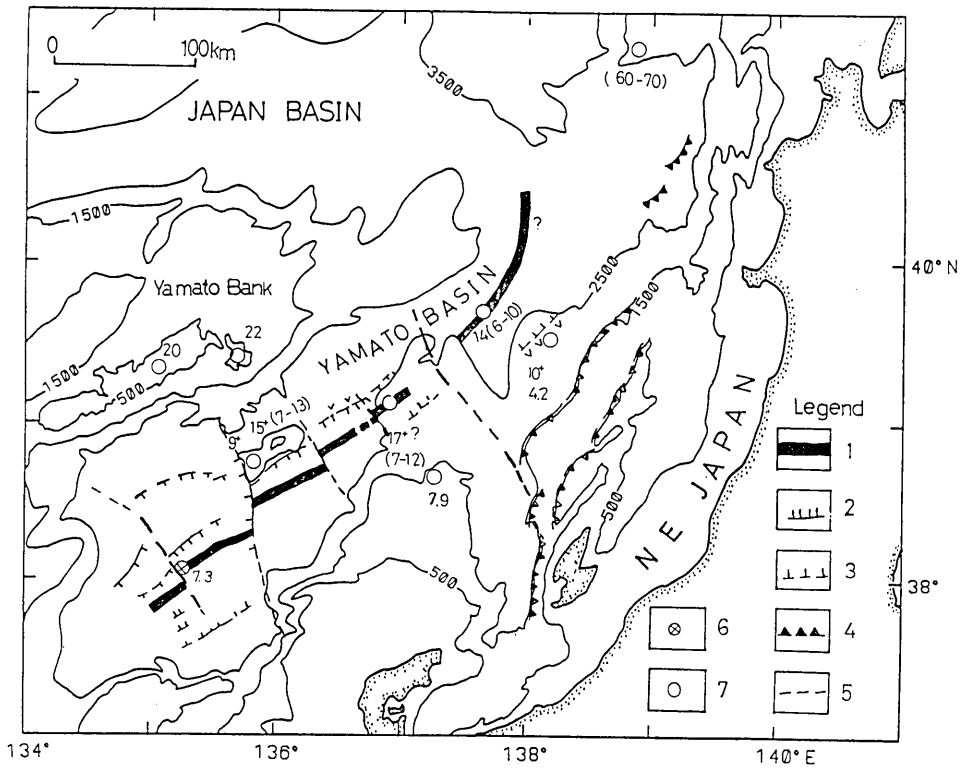

Fig. VII-20. Geotectonic map, showing the central ridge system. Absolute ages were taken from KANEOKA *et al.* (1985, 1986) and from this paper. (+) shows ^{39}Ar-^{40}Ar age and others show K-Ar ages. Legend: 1; YBR, 2; Fault. Teeth show the downthrown side, 3; Buried fault, 4; Thrust. Teeth show the upthrusted side, 5; Estimated fault, 6; Dredge site of MBB, 7; Dredge site of other rocks.

movement of the YBR. One possible explanation of both the strike slip and vertical movement along the faults is that those faults were affected by the horizontal WNW-ESE compressive strain of the area. In this case, differences in level between both sides of the knolls on the YBR were caused by thrusting components of the faults.

Those big transverse faults must have originally been generated as a transform fault associated with spreading activities along this ridge system. Then, the compressional WNW-ESE oriented stress may have prevailed since the Late Miocene Epoch around the YBR after the spreading ceased. Transform faults may have changed their nature into that of shear faults. This tendency has continued to Late Pleistocene or more recent times, intermittently. The Quaternary regional stress field clearly shows compressional features in and around the Japanese Arc (NAKAMURA and UYEDA, 1980). The continental slope off NE Japan, the eastern

marginal region of the Yamato Basin, shows active compressional features as represented in Figs. VII-17 and VII-18. Apparently active normal faults develop around the knolls standing on the YBR. They may have been formed by the surface tensional stresses that occurred by the upheaval of the basement of knolls due to WNW-ESE compression in Late Pleistocene to more recent times.

10. Summary

(1) The existence of a ridge, mostly covered with sediments, tentatively named the Yamato Basin Ridge (YBR) was recognized. The ridge may have been formed sometime during Miocene Epoch by extensive magmatism.

(2) MBB-type basalt was recovered from a part of the YBR. This supports the fact that the Yamato Basin was generated by back-arc spreading.

(3) Sedimentary structure showed that the Yamato Basin does not seem to have spread after the Miocene Epoch.

(4) Transverse faults offsetting the YBR were recognized. Those should have originated as a series of transform faults by spreading in the Miocene Epoch. They may have changed their transform nature into shear faults having thrusting components since the Pliocene Epoch.

(5) Active compressional features such as folding and thrusting exist in the continental slope off Northeast Japan. They suggest that the horizontal compressional axis is directed WNW-ESE.

References

DUNGAN, M. A., K. V. RHODES, P. E. LONG, D. P. BLANCHARD, J. C. BRANNON and K. V. RODGERS, 1978, The petrology and geochemistry of basalts from Site 396, Leg 45 and 46 of the Deep Sea Drilling Project, *Init. Rep. D.S.D.P.*, **46**, 89-113.

FRYER, P., J. M. SINTON and J. A. PHILPOTTS, 1982, Basaltic glasses from the Mariana Trough, *Init, Rep. D.S.D.P.*, **60**, 601-609.

GEOLOGICAL SURVEY OF JAPAN, 1979, Geological Investigation of the Japan Sea, *Cruise Rep.*, 13, 99p.

GEOLOGICAL SURVEY OF JAPAN, 1981, Geological Map of the Central Japan Sea, 1:1,000,000, *Marine Geology Map, Ser.* 15.

HAWKINS, J. and J. MELCIOR, 1985, Petrology of Mariana Trough and Lau Basin basalts, *J. Geophys. Res.*, **90**, 11431-11468.

HILDE, T. W. C. and J. M. WAGEMAN, 1973, Structure and origin of the Japan Sea, In P. J. Coleman (Ed.): The Western Pacific: Island Arcs, Marginal Seas, Geochemistry. University of Western Australia Press, 415-434.

HIRATA, N., H. KINOSHITA, K. SUYEHIRO, M. SUYEMASU, N. MATSUDA, T. OUCHI, H. KATAO, S. KORESAWA and S. NAGUMO, 1987, Report on DELP 1985 Cruises in the Japan Sea, Part II Seismic refraction experiment conducted in the Yamato Basin, Southeast Japan

Sea, *Bull. Earthquake Res. Inst., Univ. Tokyo*, **62**, 347-365.

HYDROGRAPHIC, DEPARTMENT, MARITIME SAFETY AGENCY, JAPAN, 1975, Ocean Sounding Chart G1407 (1:1,000,000).

HYDROGRAPHIC DEPARTMENT, MARITIME SAFETY AGENCY, JAPAN, 1980, Bathymetric Chart No. 6312, Northeast Nippon (1:1,000,000).

ISHIWADA, Y. and E. HONZA, 1984, Sedimentary basins of the Japan Sea, Origin and History of Marginal and Inland Seas, Proceedings of the 27th International Geological Congress, **23**, pp. 43-65.

KANEOKA, I., H. MEHNERT, S. ZASHU and S. KAWACHI, 1980, Pleistocene volcanic activities in the Fossa Magna region, central Japan—K-Ar age studies of the Yatsugatake volcanic chain, *Geochem. J.*, **14**, 249-257.

KANEOKA, I., Y. TAKIGAMI, K. FUJIOKA and H. SAKAI, 1985, ^{40}Ar-^{39}Ar ages of volcanic rocks dredged from the Yamato Seamount Chain, Japan Sea, *Bull. Volcanol. Soc. Japan, Ser. 2*, **30**, 296 (abstract, in Japanese).

KANEOKA, I., Y. TAKIGAMI, K. NOTSU, K. FUJIOKA and H. SAKAI, 1986, ^{40}Ar-^{39}Ar ages and Sr isotopic ratios for volcanic rocks dredged from the seamounts in the Japan Sea and their significance, The 93th Annual Meeting of the Geological Society of Japan, Abstract, 256 (in Japanese).

KARIG, D. E. and J. C. INGLER JR. (Eds.), 1975, *Init. Rep. D.S.D.P.*, **31**, 927.

KIMURA, M., 1985, Finding of the active spreading center in the Sea of Japan, *J. Geogr.* **94**, 383-387. (in Japanese).

LUDWIG, W. J., S. MURAUCHI and R. E. HOUTZ, 1975, Sediments and structure of the Japan sea, *Bull. Geol. Soc. America*, **86**, 651-664.

NAKAMURA, K. and S. UYEDA, 1980, Stress gradient in arc-back arc regions and plate subduction, *J. Geophys. Res.*, **85**, 6419-6428.

OTOFUJI, Y., T. MATSUDA and S. NOHDA, 1985a, Opening mode of the Japan Sea inferred from the paleomagnetism of the Japan Arc, *Nature*, **317**, 603-604.

OTOFUJI, Y., T. MATSUDA and S. NOHDA, 1985b, Paleomagnetic evidence for the Miocene counter-clockwise rotation of Northeast Japan—rifting process of the Japan Arc, *Earth and Planet. Sci. Lett.*, **75**, 265-277.

STEIGER, R. H. and E. JÄGER, 1977, Subcommission on geochronology: convention on the use of decay constants in geo- and cosmochronology, *Earth Planet. Sci. Lett.*, **36**, 359-362.

TAMAKI, K., 1985, Age of the Japan Sea, *J. Geogr.*, **94**, 222-237 (in Japanese with English abstract).

TAMAKI, K., 1986, Age estimation of the Japan Sea on the basis of stratigraphy, basement depth, and heat flow data, *J. Geomag. Geoelectr.*, **38**, 427-446.

TATSUMOTO, M., Y. NAKAMURA, H. KAGAMI, I. KANEOKA, H. SAKAI, Y.-K. KIM and M. KIMURA, 1986, Pb, Sr, and Nd isotopes in Japanese back-arc basalts, *EOS*, **67**, 1277 (abstract).

TOKUYAMA, H., M. SUYEMASU, K. TAMAKI, E. NISHIYAMA, S. KURAMOTO, K. SUYEHIRO, H. KINOSHITA and A. TAIRA, 1987, Report on DELP 1985 Cruises in the Japan Sea, Part III: Seismic reflection studies in the Yamato Basin and Yamato Rise areas. *Bull. Earthquake Res. Inst., Univ. Tokyo*, **62**, 367-390.

DELP 1985年度日本海研究航海報告
VII 大和海盆および付近の地形・地質

木村政昭[1]・松田高明[2]・佐藤博明[3]・兼岡一郎[4]
徳山英一[5]・倉本真一[5]・押田　淳[1]・嶋村　清[6]
玉木賢策[5]・木下　肇[7]・上田誠也[4]

1) 琉球大学理学部　2) 姫路工業大学　3) 広島大学総合科学部
4) 東京大学地震研究所　5) 東京大学海洋研究所
6) 九州東海大学農学部　7) 千葉大学理学部

本研究は日本サルベージ株式会社のチャーター船若潮丸 (493t) を用いて日本海で行われた1985年度 DELP 航海によるものである．データは精密音響測深機，多重受信式音波探査装置およびドレッジャー等を用いて得られた．その結果，埋積された海嶺と思われるものが大和海盆の中央部に位置していることがわかった．これを大和海盆海嶺と仮称した．その海嶺上に位置する小海丘である大和-85-2 海丘(仮称)からドレッジされた岩石は玄武岩であり，しかもそれは，縁海玄武岩 (MBB) とよばれるものと酷似し，K-Ar 年代は 7.3±0.5 Ma を示した．このような岩石は，日本海では今回初めて得られたものであり，これは，少なくとも大和海盆の中央部の下には縁海型の地殻が存在することを示した．また，多重受信式音波探査記録で判定される後期中新世以降の堆積層の構造は，もし，大和海盆が拡大に伴って形成されたものであるとすれば，その拡大はその堆積物が堆積する以前に行われたことを示唆している．大和海盆海嶺は，後期中新世以前に大和海盆で生じた拡大に伴う火成活動によって形成され，後期中新世に拡大軸としての活動をやめたものと推定される．

大和海盆海嶺は見かけ上いくつかの胴切断層でずれている．しかし，海嶺部のそれは垂直変位の大きいことを示している．たぶんこれらの断層は，当初は中新世の大和海盆拡大の際に形成されたトランスフォーム断層であったものが，後の (多分後期中新世～鮮新世以降) 応力場の変化によりその性質を変えたものと思われる．

また，大和海盆の東側を縁どるように位置する東北日本の大陸棚斜面上には，明かに後期更新世以降活動していると思われる褶曲や逆断層等が認められた．これらはその地域が現在ほぼ西北西―東南東方向の圧縮応力場のもとにあることと調和的である．